

Discovery of WINERED-HVS1: A metal-rich hyper-velocity star candidate ejected from the Galactic center

KOHEI HATTORI,^{1,2,3} DAISUKE TANIGUCHI,¹ TAKUJI TSUJIMOTO,¹ NORIYUKI MATSUNAGA,^{4,5} HIROAKI SAMESHIMA,⁶
SCARLET S. ELGUETA,^{7,8} AND SHOGO OTSUBO⁵

¹*National Astronomical Observatory of Japan, 2-21-1 Osawa, Mitaka, Tokyo 181-8588, Japan*

²*The Institute of Statistical Mathematics, 10-3 Midoricho, Tachikawa, Tokyo 190-8562, Japan*

³*Department of Astronomy, University of Michigan, 1085 S. University Avenue, Ann Arbor, MI 48109, USA*

⁴*Department of Astronomy, Graduate School of Science, The University of Tokyo, 7-3-1 Hongo, Bunkyo-ku, Tokyo 113-0033, Japan*

⁵*Laboratory of Infrared High-resolution spectroscopy (LiH), Koyama Astronomical Observatory, Kyoto Sangyo University, Motoyama, Kamigamo, Kita-ku, Kyoto 603-8555, Japan*

⁶*Institute of Astronomy, Graduate School of Science, The University of Tokyo, 2-21-1 Osawa, Mitaka, Tokyo 181-0015, Japan*

⁷*Departamento de Física, Universidad de Santiago de Chile, Av. Victor Jara 3659, Santiago, Chile*

⁸*Millenium Nucleus ERIS, Instituto de Estudios Astrofísicos, Universidad Diego Portales, Av. Ejército Libertador 441, Santiago, Chile*

ABSTRACT

We report the discovery of a metal-rich red giant star, WINERED-HVS1, which is a candidate for a hyper-velocity star (HVS). Its past trajectory suggests that this star may have been ejected by the Galactic supermassive black hole (SMBH; Sgr A*) about 14 Myr ago, with a modest ejection velocity of at least 500 km s⁻¹. Since WINERED-HVS1 is gravitationally bound to the Milky Way and is not necessarily young, it is not an unambiguous HVS candidate from a kinematic perspective, unlike the previously confirmed A-type main-sequence HVS known as S5-HVS1. Therefore, the chemical characterization of this star is essential for understanding its origin. Through a spectroscopic follow-up observation with Magellan/WINERED, we determined its metallicity $[\text{Fe}/\text{H}] = -0.136^{+0.040}_{-0.038}$, as well as the abundances for Na, Mg, Si, S, K, Ca, Ti, Cr, Ni, and Sr. The high metallicity value suggests that this star was ejected from the Galactic center and is unlikely to be a halo star with a radial orbit. The abundance pattern of this star—including the pattern of $[\alpha/\text{Fe}]$, $[\text{Mg}/\text{Fe}]$, $[\text{Si}/\text{Mg}]$, and $[\text{Ca}/\text{Mg}]$ —is consistent with that of the nuclear star cluster surrounding the SMBH, further supporting our view. This discovery opens a new window to look through the Galactic center environment without the hindrance of dust extinction, by using the HVSs moving in the halo region where dust extinction is minimal.

Keywords: – Hypervelocity stars (776) – High velocity stars (736) – Supermassive black holes (1663)
– Stellar abundances (1577)

1. INTRODUCTION

1.1. *Environment near the supermassive black hole in the Milky Way*

The center of the Milky Way is home to a supermassive black hole (SMBH) known as Sgr A*, which has a mass of approximately $4 \times 10^6 M_{\odot}$ (Ghez et al. 2003; Gillessen et al. 2017). Although the intense tidal forces from this SMBH hinder star formation in its immediate vicinity (Levin 2007), observations have revealed that it is surrounded by a group of stars referred to as the S-stars. These stars orbit within a radius of 0.04 pc (or 1 arcsec) and include young massive stars. If we look

further out, both the SMBH and the S-stars are contained within a nuclear star cluster (NSC) that has a half light radius of ~ 4 pc and a total mass of $2\text{--}4 \times 10^7 M_{\odot}$ (Schödel et al. 2014; Neumayer et al. 2020). The origins of these stellar components in the Galactic center remain a subject of ongoing debate (e.g., Guillard et al. 2016; Akiba et al. 2024). Studying this region is particularly challenging due to high levels of interstellar dust toward the Galactic center, which demands extensive telescope time,¹ especially in the near-infrared wave-

¹ When the manuscript of this paper was nearly ready for submission, we became aware of a study by Nandakumar et al. (2025) presenting the first results on the detailed chemical abundances of NSC stars. To maintain the independence of our analysis, we have not incorporated their findings in this paper. However, we fully acknowledge their pioneering contribution to this field. In our

Email: khattori@ism.ac.jp

Corresponding author: Kohei Hattori

lengths (Carr et al. 2000; Ramírez et al. 2000; Cunha et al. 2007; Davies et al. 2009; Pfuhl et al. 2011; Do et al. 2015; Rich et al. 2017; Feldmeier-Krause et al. 2020; Nishiyama et al. 2024; Ryde et al. 2025; Nandakumar et al. 2025). Motivated by these difficulties, here we explore an alternative approach to infer the Galactic center environment, by using stars ejected from the SMBH, known as hyper-velocity stars (HVSs).

1.2. Hyper-velocity stars as a new window to see the Galactic center environment

Hills (1988) theoretically predicted that when the SMBH disrupts a binary star system, it gravitationally captures one star (forming an S-star²), while ejecting the other star with an ejection velocity of $\sim 10^3 \text{ km s}^{-1}$, which is called an HVS.³ If such an HVS exists, it would convey important information on the chemical abundances of stars in the immediate neighbor of the SMBH (Koposov et al. 2020). A favorable property of HVSs is that they are currently moving in the halo region, where the dust extinction is negligible. Therefore, finding HVSs in the halo and characterizing their chemical abundances may provide an access to the detailed chemical properties of the Galactic center.

Brown et al. (2005) serendipitously discovered an unbound star named HVS1, which is a B-type star traveling at the heliocentric distance of $\sim 39\text{--}71 \text{ kpc}$ in the halo with a velocity of 709 km s^{-1} . Its metallicity is $[\text{Fe}/\text{H}] \simeq 0$, consistent with the Galactic center environment. Given the large velocity and the solar metallicity of this star, it is probably a HVS ejected by the SMBH, although the heliocentric distance is too uncertain that it is difficult to unambiguously trace back the orbit to the Galactic center. This discovery triggered a dedicated search for blue HVSs, resulting in discoveries of ~ 20 HVS candidates in the distant halo (Brown 2015). Later, during the course of a stellar halo survey named S5 (Li et al. 2019), Koposov et al. (2020) serendipitously discovered an unambiguous HVS dubbed S5-HVS1, which is an A-type main-sequence star moving at 9 kpc from the Sun with a velocity of 1755 km s^{-1} . Due to its relative proximity from the Sun, its orbit can be traced back to the Galactic center with a small uncertainty. S5-HVS1 is currently the only unambiguous HVS from the Galactic center. Although the metallicity is estimated to be $[\text{Fe}/\text{H}] = 0.29 \pm 0.08$ (Koposov et al. 2020), its detailed chemical abundances (such as α -abundance) are yet to be determined, because this A-type star has weak metal lines due to its high temperature.

forthcoming paper (Taniguchi et al. in prep), we will discuss the implications from Nandakumar et al. (2025) in some detail.

² The formation process of S-stars is not fully understood, and there may be multiple channels to form these stars. Binary disruption is one of the possible mechanisms to form S-stars.

³ In this paper, we define HVSs as those stars ejected from the Galactic center, regardless of their velocities.

The ejection rate of HVSs is estimated to be one per $\sim 10^4$ years (Zhang et al. 2013; Brown 2015; Marchetti et al. 2018; see also Verberne et al. 2024 for a recent claim of lower ejection rate). If HVSs travel with a velocity of $\sim 10^3 \text{ km s}^{-1}$, a simple calculation suggests that there are $\sim 10^4$ HVSs within 100 kpc from the Galactic center (see Section 4.5 of Brown 2015; see also Marchetti et al. 2018). Considering that the stellar halo contains $\sim 10^9$ stars (Deason et al. 2019), only one in 10^5 of stars in the halo region is a HVS. The rarity of HVSs means that we need to search for HVSs from a large catalog. Following the major data releases from Gaia, namely Gaia DR2, EDR3, and DR3 (Gaia Collaboration et al. 2016, 2018, 2021, 2023), many authors have attempted to find HVSs from Gaia’s large 6D position-velocity catalog (Hattori et al. 2018a; Marchetti et al. 2019; Marchetti 2021; Marchetti et al. 2022a; Li et al. 2021). Although they discovered some fast-moving stars, none of them are unambiguous HVSs. From kinematical point of view, their ‘high’-velocity or ‘extreme’-velocity stars do not include unambiguous and unbound HVSs from the Galactic center. This is partly because the HVSs are very rare and partly because the stellar halo is dominated by halo stars with nearly radial orbits (Belokurov et al. 2018; Helmi et al. 2018).

Although previous kinematical searches for HVSs in the Gaia catalog did not result in discoveries of unambiguous HVSs, we still have a hope to find HVSs. Since typical stars near the Galactic center are much more metal-rich than field halo stars, HVSs should stand out when viewed in the chemistry space. Recently, extremely low-resolution stellar spectra named Gaia XP spectra were published for 219 million stars as part of the Gaia DR3 (De Angeli et al. 2023; Montegriffo et al. 2023). The Gaia XP spectra have a revolutionary impact on the search for HVSs. By using the Gaia XP spectra, Hattori (2025) estimated the metallicity $[\text{M}/\text{H}]_{\text{XP}}$ and α -abundance $[\alpha/\text{M}]_{\text{XP}}$ for 48 million stars in the low dust extinction regions (see Table 7). This is the largest catalog of stars for which both metallicity and α -abundance are available. In this paper, we combine the chemical data from Hattori (2025) and the position/velocity data from Gaia DR3 to hunt for HVSs ejected from the Galactic center. By using Magellan/WINERED, we conduct a follow-up observation for the most metal-rich candidate, WINERED-HVS1, and we conclude that it is the most promising HVS candidate based on its detailed chemical abundances.

1.3. Structure of this paper

This paper is organized as follows. In Section 2, we describe the strategy to find HVSs. In Section 3, we describe the data used in this paper. In Section 4, we describe our assumptions on the Solar position and velocity. In Section 5, we first use the backward orbit integration to obtain 74 kinematically-selected HVS candidates. Then we select 22 metal-rich HVS candidates by addi-

tionally using their chemical properties. We conducted a follow-up observation for the most metal-rich HVS candidate (WINERED-HVS1) with Magellan/WINERED, as described in [Section 6](#). In [Section 7](#), we describe the kinematical and chemical properties of the 22 HVS candidates and argue that WINERED-HVS1 is the most promising candidate of a HVS ejected from the Galactic center. We compare the detailed chemistry of this star to discuss its origin from chemical point of view. In [Section 8](#), we summarize our paper.

2. STRATEGY TO FIND HVS CANDIDATES

The aim of this paper is to find HVSs that were recently (up to 200 Myr in the past) ejected from the Galactic center, by the dynamical interaction with the SMBH, Sgr A*. In this paper, we do not restrict ourselves to those HVSs that are unbound to the Galactic potential. As HVSs are no longer located in the Galactic center region, finding candidates of HVSs in the Gaia catalog (or in any given sample of stars) requires us to have a reliable model of the stellar orbits in the past. To build such a model, we need to know

- (i) the Galactic potential;
- (ii) the Solar position and velocity with respect to the Galactic center; and
- (iii) the stellar position and velocity relative to the Sun.

If we had the perfect knowledge on (i)-(iii), finding HVSs would be straightforward because we would just need to trace the orbit backward in time and to find stars that ‘penetrate’ through the Galactic center. In reality, however, we have a limited understanding of (i)-(iii) mentioned above. To handle these uncertainties, we search for HVS candidates with four methods (methods A, B, C, and D) shown in [Table 1](#). We combine the results from these search methods to obtain the final, robust sample of HVS candidates.

Regarding the uncertainty associated with (i), we use two widely-used Galactic potential models in this paper (see [Table 1](#)). The fiducial model is an axisymmetric model explored by [McMillan \(2017\)](#), and the secondary model is a barred potential explored by [Portail et al. \(2017\)](#) in which the bar’s pattern speed is assumed to be $\Omega_{\text{bar}} = 39 \text{ km s}^{-1} \text{ kpc}^{-1}$ (in the prograde direction). By using these two potentials, we can search for HVS candidates that are robust against the specific choice of the adopted potential. Also, in this paper we restrict ourselves to find HVSs that are recently ejected (within 200 Myr in the past) (a) unbound HVSs or (b) bound HVSs that have not experienced disk crossing after ejection. Because our inference on the stellar orbits becomes less reliable if we adopt longer integration time backward in time (or longer ‘flight time’), our choice of short integra-

Table 1. Four methods to kinematically search for HVS candidates

(1)	(2)	(3)
Search method	Potential model	Assumed (R_0, V_\odot)
A (fiducial)	McMillan (2017)	Fix (R_0, V_\odot)
B	McMillan (2017)	Vary (R_0, V_\odot)
C	Portail et al. (2017)	Fix (R_0, V_\odot)
D	Portail et al. (2017)	Vary (R_0, V_\odot)

NOTE— (1) Names of the search methods. Method A is considered as the fiducial analysis. (2) Assumed models of the Galactic gravitational potential. The model in [McMillan \(2017\)](#) is axisymmetric. The model in [Portail et al. \(2017\)](#) is a barred potential model, for which we assume a constant pattern speed of the bar ($\Omega_{\text{bar}} = 39 \text{ kpc km s}^{-1}$). (3) The assumptions on the Solar position and velocity. (See [Section 4](#) for further details.)

tion time minimizes the mis-classification of non-HVSs as HVS candidates.⁴

Regarding the uncertainty associated with (ii), we try two assumptions on the Solar position and velocity, $(\mathbf{x}_\odot, \mathbf{v}_\odot)$, for each of the adopted potential models as shown in [Table 1](#). For methods A and C, we fix the Solar Galactocentric radius $R_0 = 8.277 \text{ kpc}$ and the Galactocentric azimuthal velocity of the sun, $V_\odot = 251.5 \text{ km s}^{-1}$, while for methods B and D, we try different set of (R_0, V_\odot) each time we compute the stellar orbits, as detailed in [Section 4](#). To the best of our knowledge, this is the first time the uncertainties in (R_0, V_\odot) are taken into account in finding HVS candidates.⁵ Our investigation allows us to check how our search of HVSs are sensitive to the assumptions on R_0 and V_\odot (or \mathbf{x}_\odot and \mathbf{v}_\odot).

Regarding the uncertainty associated with (iii), for each star, we draw $N_{\text{MC}} = 10^4$ Monte Carlo samples of the stellar position and velocity (relative to the Sun) that reflect the observational uncertainty (see [Section 3.2](#)). For each star, we use N_{MC} orbits that are integrated backward in time for up to 200 Myr under the assumed potential. By using these orbits, we select stars that may have been ejected from the Galactic center recently.

⁴ In this paper, we choose a short integration time of 200 Myr, which makes our work distinct from [Marchetti et al. \(2022b\)](#), who integrated the orbits for as long as 1 Gyr to search for HVS candidates. In principle, we can relax our assumption of short integration time and investigate the (bound) HVS candidates that have experienced one or two disc crossings after the ejection from the Galactic center. However, we stick to this short integration time because we have found an interesting HVS candidate WINERED-HVS1 under our current assumption.

⁵ There has been an attempt to determine (R_0, V_\odot) by using an HVS ([Koposov et al. 2020](#)) with a method explored by [Hattori et al. \(2018b\)](#).

3. STELLAR DATA

Here we describe the data set we use in this paper. In [Section 3.1](#), we describe how we construct the sample of metal-rich stars from which we search for candidates of HVSSs. In [Section 3.2](#), we describe how we draw a Monte Carlo sample of the observed quantities for each star, which will be used in the subsequent analysis. Our notations for astrometric quantities, such as ϖ , μ_{α^*} , μ_{δ} , or v_{los} are summarized in [Table 7](#).

3.1. Selection of data

We construct the catalog of metal-rich stars by using the position-velocity data in Gaia DR3 catalog ([Gaia Collaboration et al. 2023](#)), the photometric distance from [StarHorse](#) catalog ([Anders et al. 2022](#)), and the chemical abundance catalog from [Hattori \(2025\)](#).

First, from the main catalog (`gaia_source`) of the Gaia DR3, we select stars with the following conditions

- `parallax_over_error` ($= \varpi/\sigma_{\varpi}$) > 5 ,
- `radial_velocity` (v_{los}) is not Null,
- $v_{\text{tot}}^{\text{point-estimate}} > 200 \text{ km s}^{-1}$.

Here, $v_{\text{tot}}^{\text{point-estimate}}$ is the point-estimate of the total velocity in the Galactocentric rest frame. The lower limit on $v_{\text{tot}}^{\text{point-estimate}}$ is set for (i) excluding most of the disk stars; and (ii) excluding halo stars with low velocity. In computing $v_{\text{tot}}^{\text{point-estimate}}$, we derive the point-estimate of the heliocentric distance to the star by $d = 1/\varpi$. This treatment is valid because we restrict ourselves to stars with good parallax measurements. Also, in computing $v_{\text{tot}}^{\text{point-estimate}}$, we assume the Galactocentric position and velocity of the sun as described in [Section 4.1](#).

Secondly, we cross-match the catalog with the [StarHorse](#) catalog ([Anders et al. 2022](#)) to obtain photometric distance information. As described in [Section 3.2](#), we will use the 5th and 95th percentile values from the probability distribution of the photometric distance for each star, which are denoted as `dist05` and `dist95`.

Finally, we cross-match the catalog with the chemical abundance catalog⁶ in [Hattori \(2025\)](#). To reduce the contamination from halo stars (i.e., those stars that are not ejected from the Galactic center), we select stars with $[\text{M}/\text{H}]_{\text{XP}} > -1$ and `bool_flag_cmd_good = True`. The remaining $\sim 6,600,000$ stars will be analyzed in the following section.

3.2. Monte Carlo realizations of the observed quantities of the star

Here we describe how we generate Monte Carlo realizations of the position and velocity of the stars that reflect the uncertainties in the observed quantities. In

the following, we focus on the procedure for i th star in our catalog.

For i th star in our catalog, we draw $N_{\text{MC}} = 10^4$ realizations of the observable vector $(\alpha, \delta, d, \mu_{\alpha^*}, \mu_{\delta}, v_{\text{los}})$ by taking into account the associated error distribution, in a similar manner as in [Hattori et al. \(2023\)](#). We denote the j th realization of the observable vector (for star i) as

$$\mathbf{q}_{ij} = (\alpha^{(ij)}, \delta^{(ij)}, d^{(ij)}, \mu_{\alpha^*}^{(ij)}, \mu_{\delta}^{(ij)}, v_{\text{los}}^{(ij)}). \quad (1)$$

We neglect the tiny observational uncertainty in the sky coordinate, and thus we set $(\alpha^{(ij)}, \delta^{(ij)})$ to the observed right ascension and declination in Gaia DR3 catalog. We draw the heliocentric distance $d^{(ij)}$ from the uniform distribution between `dist05` $< d <$ `dist95`, where `dist05` and `dist95` are the 5th and 95th percentile values of the heliocentric distance of i th star taken from the [StarHorse](#) catalog. We draw the proper motion vector $(\mu_{\alpha^*}^{(ij)}, \mu_{\delta}^{(ij)})$ from the error distribution in Gaia DR3 catalog, by taking into account the correlation between the two proper motion components. We do not take into account the correlation between the parallax (inverse of the distance) and the proper motion. We draw the line-of-sight velocity $v_{\text{los}}^{(ij)}$ from the error distribution in Gaia DR3 catalog.

After these procedures, for each star i , we obtain $N_{\text{MC}} = 10^4$ sets of phase-space vector \mathbf{q}_{ij} . The same sets of \mathbf{q}_{ij} will be analyzed with different assumptions on the Galactic potential model or on the values of (R_{\odot}, V_{\odot}) (see [Table 1](#)).

4. THE POSITION AND VELOCITY OF THE SUN

We use a right-handed Cartesian coordinate system in which the Galactic plane is the (x, y) -plane, and z is directed to the North Galactic Pole. The Sun is located at $\mathbf{x}_{\odot} = (x, y, z)_{\odot} = (-R_{\odot}, 0, z_{\odot})$ and its velocity is $\mathbf{v}_{\odot} = (v_x, v_y, v_z)_{\odot} = (U_{\odot}, V_{\odot}, W_{\odot})$. We fix $(\mathbf{x}_{\odot}, \mathbf{v}_{\odot})$ in methods A and C, while we vary these quantities in methods B and D.

4.1. Fixed Solar position and velocity: Methods A and C

For methods A and C (see [Table 1](#)), we fix the Solar position and velocity throughout the analysis. Namely, we assume $z_{\odot} = 0.0208 \text{ kpc}$ ([Bennett & Bovy 2019](#)) and $(U_{\odot}, W_{\odot}) = (11.1, 7.25) \text{ km s}^{-1}$ ([Schönrich et al. 2010](#)). Also, we fix $(R_{\odot}, V_{\odot}) = (8.277 \text{ kpc}, 251.5 \text{ km s}^{-1})$, based on recent measurements ([GRAVITY Collaboration et al. 2022](#); [Reid & Brunthaler 2020](#)).

4.2. Varied Solar position and velocity: Methods B and D

For methods B and D (see [Table 1](#)), we take into account the uncertainties in the Solar position and velocity. For this aim, we prepare $N_{\text{MC}} = 10^4$ combinations of

⁶ <https://zenodo.org/records/10902172>

$(\mathbf{x}_\odot^{(j)}, \mathbf{v}_\odot^{(j)})$, where $j = 1, \dots, N_{\text{MC}}$, in the following manner. We assume the same fixed values for (z_0, U_\odot, W_\odot) as before. For (R_0, V_\odot) , in contrast, we use $N_{\text{MC}} = 10^4$ pairs of values, $\{(R_0^{(j)}, V_\odot^{(j)}) \mid j = 1, \dots, N_{\text{MC}}\}$, which are drawn from the following procedure:

$$R_0^{(j)} \sim \mathcal{N}(8.277, 0.1) \text{ kpc}, \quad (2)$$

$$\Omega_{\text{SgrA}}^{(j)} \sim \mathcal{N}(-6.411, 0.008) \text{ mas yr}^{-1}, \quad (3)$$

$$V_\odot^{(j)} = k R_0^{(j)} (-\Omega_{\text{SgrA}}^{(j)}), \quad (4)$$

with $k = 4.74047 \text{ km s}^{-1} \text{ kpc}^{-1} (\text{mas yr}^{-1})^{-1}$. Here, $a \sim \mathcal{N}(m, s)$ denotes that a is drawn from a Gaussian distribution with mean m and standard deviation s . In this procedure, we adopt the recent estimate of $R_0 = 8.277 \text{ kpc}$ (GRAVITY Collaboration et al. 2022) and the estimate of the uncertainty in R_0 of 0.1 kpc from Bland-Hawthorn & Gerhard (2016). We assume that the apparent angular motion of the Sgr A* in the Galactic longitude direction, $\Omega_{\text{SgrA}} = -6.411 \pm 0.008 \text{ mas yr}^{-1}$ (Reid & Brunthaler 2020), corresponds to the Solar reflex motion. The minus sign in equation (4) is introduced because what we want is not the motion of Sgr A* with respect to the Sun but the motion of the Sun with respect to Sgr A*.

5. SEARCH FOR HVS CANDIDATES

5.1. Backward orbit integration

Here we describe how we find the HVS candidates. To be specific, we describe how we judge whether i th star in our catalog has a non-trivial probability of having been ejected by the SMBH.

From Section 3.2, we have the position-velocity data of i th star relative to the Sun, represented by N_{MC} Monte Carlo samples. For j th Monte Carlo sample, we have the 6D observable vector \mathbf{q}_{ij} defined in equation (1). We convert \mathbf{q}_{ij} to the Galactocentric Cartesian position and velocity vector $(\mathbf{x}_{ij}, \mathbf{v}_{ij})$, by using the assumed Solar position and velocity $(\mathbf{x}_\odot, \mathbf{v}_\odot)$. Here, we use the fixed value of $(\mathbf{x}_\odot, \mathbf{v}_\odot)$ in methods A and C, while we use $(\mathbf{x}_\odot, \mathbf{v}_\odot) = (\mathbf{x}_\odot^{(j)}, \mathbf{v}_\odot^{(j)})$ in methods B and D. Then, from the current-day position-velocity $(\mathbf{x}_{ij}, \mathbf{v}_{ij})$, we integrate the orbit backward in time for 200 Myr (from the current epoch $t = 0$ to $t = -200 \text{ Myr}$) in the model potential of the Milky Way. As shown in Table 1, we use McMillan (2017) for methods A and B, while we use Portail et al. (2017) for methods C and D.

If j th orbit of i th star crosses the disk plane at $-200 \text{ Myr} < t < 0 \text{ Myr}$, we record the orbital properties when it crosses the disk plane, namely the disk-crossing time, disk-crossing position, and disk-crossing velocity (in a similar manner as in Hattori et al. 2019). In this paper, we interpret these quantities as the disc-ejection time t_{ej} , disk-ejection position $\mathbf{x}_{\text{ej}} = (x_{\text{ej}}, y_{\text{ej}}, 0)$, and disk-ejection velocity $\mathbf{v}_{\text{ej}} = (v_{x,\text{ej}}, v_{y,\text{ej}}, v_{z,\text{ej}})$, re-

spectively. We define the flight time as

$$t_{\text{flight}} = -t_{\text{ej}}, \quad (5)$$

following the convention in Brown (2015). We define the ejection radius as

$$r_{\text{ej}} = (x_{\text{ej}}^2 + y_{\text{ej}}^2)^{1/2}. \quad (6)$$

Also, we define the magnitude of ejection velocity as

$$v_{\text{ej}} = (v_{x,\text{ej}}^2 + v_{y,\text{ej}}^2 + v_{z,\text{ej}}^2)^{1/2}. \quad (7)$$

We note that the assumed potential model of McMillan (2017) (or Portail et al. 2017) does not contain the compact components near the Galactic center (such as the contributions from the SMBH, NSC, or NSD). Thus, the value of v_{ej} computed in our analysis does not include the effect from these compact components. For example, suppose that a certain HVS candidate has $v_{\text{ej}} = 600 \text{ km s}^{-1}$. In this case, it does not mean that the star was ejected by the SMBH with this ejection velocity. Rather, 600 km s^{-1} corresponds to the velocity of the HVS candidate when it escapes from the gravitational influence from the SMBH (say a few pc from the Galactic center).

5.2. Kinematically-selected HVS candidates

For each method (methods A-D), we conduct the backward orbit integration and derive the disc ejection location and velocity. Then we consider a star as a ‘kinematically-selected HVS candidate’ if at least one of the following conditions are satisfied:

- (Condition 1) For star i , count the number of Monte Carlo orbits that satisfy $r_{\text{ej}} < 50 \text{ pc}$, $v_{\text{ej}} > 500 \text{ km s}^{-1}$, and $t_{\text{flight}} < 200 \text{ Myr}$. If more than 1% of Monte Carlo orbits satisfy these conditions, we regard star i as a HVS candidate.
- (Condition 2) For star i , count the number of Monte Carlo orbits that satisfy $r_{\text{ej}} < 200 \text{ pc}$, $v_{\text{ej}} > 500 \text{ km s}^{-1}$, and $t_{\text{flight}} < 200 \text{ Myr}$. If more than 25% of Monte Carlo orbits satisfy these conditions, we regard star i as a HVS candidate.

These conditions are not mutually exclusive, so a star may satisfy both (Condition 1) and (Condition 2). (The number of kinematically-selected HVS candidates will be described in Section 5.3.)

The idea behind (Condition 1) and (Condition 2) is to try not to miss the genuine, recently-ejected HVSs in our sample. For example, suppose that we are confident on the assumed gravitational potential model and the Solar position and velocity. In this case, the uncertainty in the stellar orbit arises mainly from the uncertainty in the current-day position and velocity of the star. Since we have prepared a large number of Monte Carlo orbits per star, we believe that at least a small fraction of

the Monte Carlo orbits are close to the genuine orbits and have small r_{ej} . Therefore, (Condition 1) works well to select HVS candidates.

In contrast, suppose that we are not very confident on the assumed gravitational potential model or the Solar position and velocity. In this case, a genuine, recently-ejected HVS may not have very small r_{ej} if the assumed potential is not a good approximation to the actual Milky Way potential. In order to investigate how the wrongly-assumed potential models affects the value of r_{ej} , we conduct a simple test. Here, we eject HVSs from the Galactic center (with ejection velocity of $\sim 600 \text{ km s}^{-1}$ and flight time of $\sim 30 \text{ Myr}$) assuming a realistic potential model (the model in [McMillan 2017](#)) and rewinding the orbit backward in time in another realistic potential (the model in [Portail et al. 2017](#)) until the disc crossing. As a result, we find that $r_{\text{ej}} < 200 \text{ pc}$ is satisfied for the majority ($\sim 80\%$) of simulated HVSs. Our simplified test suggests that a genuine, recently-ejected HVS probably satisfy $r_{\text{ej}} < 200 \text{ pc}$. Therefore, (Condition 2) works well to select HVS candidates.

5.3. Number of kinematically-selected HVS candidates

[Table 2](#) summarizes the number of kinematically-selected HVS candidates when methods A, B, C, and D are adopted. This table shows that the kinematically-selected HVS candidates mainly depend on the assumed potential and only weakly depend on the Solar position and velocity. For example, among 141 candidates found in method A (row 1 in [Table 2](#)), 133 candidates (94%) are also considered as candidates in method B; and among 239 HVS candidates found in method C (row 3), 230 candidates (96%) are also considered as candidates in method D.⁷ In contrast, among 141 candidates found in method A (row 1), 76 candidates (54%) are also considered as candidates in method C; and among 141 HVS candidates found in method B (row 2), 79 candidates (56%) are also considered as candidates in method D.⁸ Given that the list of kinematically-selected HVS candidates depends on the assumed potential, it is reassuring to note that 74 stars are regarded as kinematically-selected HVS candidates for all the methods we explored (row 19 in [Table 2](#)). It turned out that all of these 74 candidates are bound to the Milky Way. In the following, we will analyze these 74 kinematically-selected HVS candidates in more detail.

5.4. Further pruning of HVS candidates with chemistry

From the 74 kinematically-selected HVS candidates, we further select 22 metal-rich HVS candidates as sum-

⁷ The sum of the number of candidates for ABxx, ABCx, ABxD, and ABCD in [Table 2](#) is 133. The sum for xxCD, AxCD, xBCD, and ABCD is 230.

⁸ The sum of the number of candidates for AxCx, ABCx, AxCD, and ABCD in [Table 2](#) is 76. The sum for xBxD, ABxD, xBCD, and ABCD is 79.

Table 2. Number of HVS candidates

(1)	(2)	(3)	(4)
Row	Methods	N	Description
1	A	141	# of candidates found by method A
2	B	141	# of candidates found by method B
3	C	239	# of candidates found by method C
4	D	243	# of candidates found by method D
5	Axxx	6	# of candidates found by A only
6	xBxx	5	# of candidates found by B only
7	xxCx	7	# of candidates found by C only
8	xxxD	10	# of candidates found by D only
9	ABxx	56	# of candidates found by A and B only
10	AxCx	1	# of candidates found by A and C only
11	AxxD	0	# of candidates found by A and D only
12	xBCx	1	# of candidates found by B and C only
13	xBxD	0	# of candidates found by B and D only
14	xxCD	153	# of candidates found by C and D only
15	ABCx	0	# of candidates found by A, B, and C only
16	ABxD	3	# of candidates found by A, B, and D only
17	AxCD	1	# of candidates found by A, C, and D only
18	xBCD	2	# of candidates found by B, C, and D only
19	ABCD	74	# of candidates found by all the methods

NOTE— (1) Row number. (2) Methods used to search for HVS candidates. The character x is used as a space holder indicating the method not used. (3) Number of HVS candidates. (4) Description of the adopted method(s). In rows 1-4, we show the number of candidates that are found by using each of the methods A-D. In rows 5-18, we show the number of candidates that only appear in a particular combinations of the methods. In row 19, we show the number of candidates (74 stars) that appear in all the methods A-D. These 74 stars are HVS candidates that are robust against the choice of the gravitational potential or the assumptions on the solar position/velocity.

marized in [Fig. 1](#). Here we describe the selection process of these 22 stars.

First, we remove 4 RR Lyrae stars by using the RR Lyrae catalog in [Clementini et al. \(2023\)](#) and the SIMBAD data base. Among the remaining 70 stars, 10 stars have reliable chemical information from either APOGEE DR17 ([Abdurro'uf et al. 2022](#)), GALAH DR4 ([Buder et al. 2024](#)), RAVE DR6 ([Steinmetz et al. 2020](#)), LAMOST DR9 v2.0 ([Zhao et al. 2012](#)). Among these stars, 9 stars satisfy⁹ $[\text{Fe}/\text{H}]_{\text{spec}} > -1$. We refer to these stars as ‘spectroscopically confirmed metal-rich HVS candidates’ and label them as mrHVSspec1-9. All of these HVS candidates are red giants.

Then, for the 60 stars without spectroscopic chemical abundances, we use the chemical abundances ($[\text{M}/\text{H}]_{\text{XP}}$, $[\alpha/\text{M}]_{\text{XP}}$) derived from extremely low-resolution Gaia XP spectra by using machine-learning models ([Hattori 2025](#)). We select 13 stars that satisfy the quality crite-

⁹ Throughout this paper, $[\text{X}/\text{Y}]_{\text{spec}}$ denotes the spectroscopic measurements of $[\text{X}/\text{H}]$. See [Table 7](#).

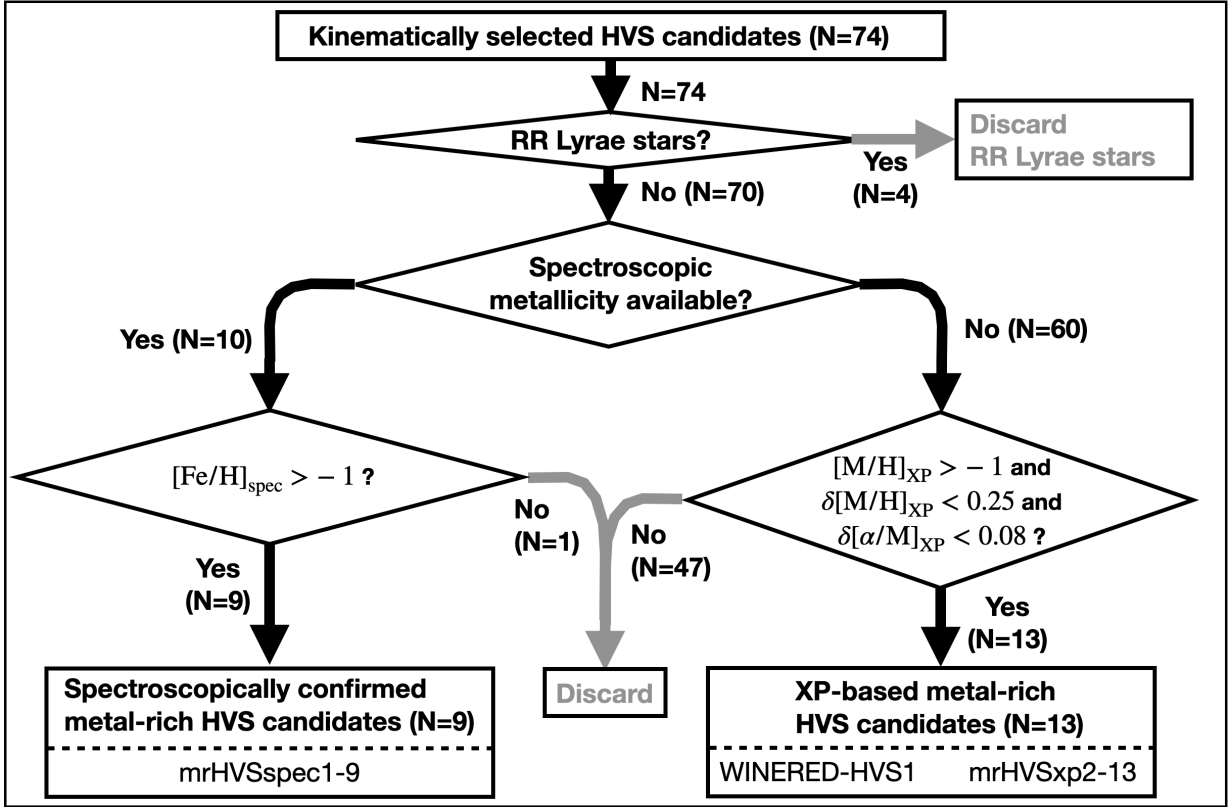


Figure 1. Flow chart to chemically select 22 metal-rich HVS candidates from the 74 kinematically selected HVS candidates. We refer to the 9 candidates with spectroscopic chemistry from literature as ‘spectroscopically confirmed metal-rich HVS candidates.’ We refer to the remaining 13 candidates as ‘XP-based metal-rich HVS candidates.’ The most metal-rich candidate, WINERED-HVS1, is among the XP-based metal-rich HVS candidates.

ria in [Hattori \(2025\)](#), while showing $[M/H]_{XP} > -1$.¹⁰ We refer to these stars as ‘XP-based metal-rich HVS candidates.’ We label the most metal-rich candidate as WINERED-HVS1, while we label the rest of them as mrHVSxp2-13. Again, all of the XP-based metal-rich HVS candidates are red giants.

As can be inferred from the unique name convention for WINERED-HVS1, we regard this star different from other HVS candidates because it has intriguing chemical properties. Its XP-based metallicity, $[M/H]_{XP} = -0.23$, is higher than any other HVS candidates analyzed in this paper. Also, its α -abundance, $[\alpha/M]_{XP} = 0.06$, is one of the least α -enhanced stars in our HVS candidates. At face value, the metal-rich and α -poor nature of WINERED-HVS1 is reminiscent of the stellar population near the Galactic center region. We did a follow-up observation of this star with Magellan/WINERED and spectroscopically confirmed the metal-rich and α -poor nature of this star (see [Section 6](#)). Kinematics and chem-

istry of the 22 HVS candidates, including WINERED-HVS1, will be discussed in [Section 7](#).

6. SPECTROSCOPIC OBSERVATION OF A HYPER-VELOCITY STAR CANDIDATE WINERED-HVS1

We obtained a near-infrared YJ -band high-resolution spectrum of WINERED-HVS1 using the WINERED spectrograph (0.90–1.35 μm with $R = 28,000$; [Ikeda et al. 2022](#)) attached to the Magellan Clay Telescope on June 6th 2023. We performed the ABBA nodding with 600sec exposures. With the J -band magnitude of 12.69 (2MASS; [Cutri et al. 2003](#)), the resultant signal-to-noise ratio (S/N) per pixel is 40–115 for the Y band (0.97–1.09 μm) and 25–90 for the J band (1.15–1.32 μm). We also observed a telluric-standard A0V star, HD 170115, with a sufficient S/N of 200–400. The raw data was reduced using the WINERED Automatic Reduction Pipeline (WARP version 3.8.7; [Hamano et al. 2024](#)), and telluric lines were removed with the standard star using the method described by [Sameshima et al. \(2018\)](#). Then the line-of-sight velocity was determined using the cross-correlation function between the observed and synthesized spectra, and the wavelengths were adjusted to the standard-air scale at

¹⁰ We have already applied the cut $[M/H]_{XP} > -1$ in [Section 3](#). We show this cut also in [Fig.1](#) just to emphasize that XP-based metal-rich HVS candidates do not include metal-poor stars.

Table 3. Kinematical properties of our HVS candidates

(1)	(2)	(3)	(4)	(5)	(6)	(7)	(8)	(9)	(10)	(11)
Name	DR3 source_id	($f_{50 \text{ pc}}, f_{200 \text{ pc}}$)	r_{ej}	v_{ej}	t_{flight}	(x, y, z)	(r, R)	(v_x, v_y, v_z)	(v_r, v_R, v_ϕ)	v
			pc	km s ⁻¹	Myr	kpc	kpc	km s ⁻¹	km s ⁻¹	km s ⁻¹
HVSs pec1	1364083369852936576	[0.2525, 0.9708]	0	535	26	[-7.60, +2.69, +1.60]	[8.22, 8.06]	[-175, +62, -7]	[+181, +186, -0]	186
HVSs pec2	3894254612584073472	[0.0218, 0.1212]	1	578	22	[-8.04, -1.21, +2.82]	[8.60, 8.13]	[-265, -40, +60]	[+273, +268, -0]	275
HVSs pec3	650895057975204864	[0.0359, 0.0943]	1	606	15	[-4.09, -1.67, -5.26]	[6.87, 4.42]	[-221, -90, -258]	[+351, +238, +0]	351
HVSs pec4	2694242193191538816	[0.1053, 0.8001]	1	533	24	[-7.54, +1.29, -1.09]	[7.73, 7.65]	[-197, +34, +16]	[+196, +200, +0]	201
HVSs pec5	6137389419947219584	[0.0000, 0.2973]	54	521	23	[-4.44, -5.08, +2.37]	[7.15, 6.75]	[-122, -136, +21]	[+180, +183, -3]	184
HVSs pec6	5467370673479835904	[0.0001, 0.3035]	46	571	21	[-8.28, -1.63, +0.74]	[8.47, 8.44]	[-268, -55, -10]	[+272, +274, +2]	274
HVSs pec7	6692069426721736832	[0.0504, 0.0536]	5	501	11	[-2.76, +0.21, -2.83]	[3.96, 2.77]	[-186, +14, -153]	[+239, +186, +1]	241
HVSs pec8	3552388581761193728	[0.0339, 0.1519]	3	556	25	[-8.26, -2.33, +1.72]	[8.76, 8.59]	[-219, -62, +7]	[+224, +227, +0]	227
HVSs pec9	3657091157063641344	[0.0120, 0.1198]	2	543	21	[-6.33, -1.04, +3.20]	[7.17, 6.42]	[-214, -35, +71]	[+226, +217, -0]	228
WINERD-HVS1	6434696676903108864	[0.0310, 0.4957]	16	537	14	[-4.44, -2.30, -2.18]	[5.45, 5.00]	[-232, -122, -76]	[+270, +262, +1]	273
HVSxp2	4548672495942395264	[0.1131, 0.4637]	0	544	15	[-4.75, +2.81, +1.89]	[5.84, 5.52]	[-234, +138, +54]	[+274, +271, +0]	277
HVSxp3	6173750574418020352	[0.0469, 0.0564]	1	502	25	[-3.60, -3.97, +3.69]	[6.51, 5.36]	[-83, -92, +40]	[+125, +124, -0]	130
HVSxp4	4572287497444895104	[0.0914, 0.3728]	1	556	17	[-5.44, +2.72, +2.74]	[6.67, 6.09]	[-233, +117, +81]	[+271, +261, +0]	273
HVSxp5	6307609625404677376	[0.0147, 0.1091]	7	540	13	[-2.82, -1.46, +4.01]	[5.12, 3.18]	[-164, -84, +200]	[+272, +185, -0]	272
HVSxp6	5765626877690171904	[0.0034, 0.2743]	7	518	23	[-6.41, -2.59, -1.46]	[7.06, 6.91]	[-168, -68, +10]	[+175, +181, -0]	182
HVSxp7	6773393846499438464	[0.0349, 0.1637]	3	503	77	[-2.73, +1.92, -1.81]	[3.80, 3.34]	[+120, -84, +223]	[-235, -146, -0]	267
HVSxp8	6425246443181463680	[0.0188, 0.1082]	2	532	18	[-3.37, -3.02, -4.16]	[6.15, 4.53]	[-136, -122, -133]	[+225, +183, +0]	226
HVSxp9	4501932497166815360	[0.0009, 0.2663]	30	547	18	[-1.69, +6.03, +2.79]	[6.85, 6.26]	[-64, +232, +71]	[+249, +241, -1]	251
HVSxp10	1497611497903517056	[0.0534, 0.5141]	2	568	23	[-8.08, +0.86, +2.45]	[8.48, 8.12]	[-253, +27, +41]	[+255, +254, +0]	257
HVSxp11	1329060763412103808	[0.0159, 0.3891]	8	579	19	[-6.42, +2.75, +3.42]	[7.78, 6.98]	[-251, +107, +101]	[+289, +273, +1]	291
HVSxp12	5130376441238310016	[0.0426, 0.2071]	0	575	33	[-10.16, -0.71, -4.35]	[11.07, 10.18]	[-205, -14, -57]	[+212, +206, +0]	214
HVSxp13	3929723865560075776	[0.0238, 0.1063]	2	598	25	[-7.28, -1.31, +6.65]	[9.95, 7.39]	[-220, -39, +177]	[+284, +223, -0]	285

NOTE—(1) Name of the metal-rich HVS candidates. Stars named mrHVSs pec1-9 are HVS candidates for which we have spectroscopic abundance information from publicly available data. For WINERD-HVS1, we have spectroscopic abundance information from our follow-up observations with Magellan/WINERD. Stars named mrHV Sxp2-15 are HVS candidates for which we have the abundance information from the Gaia XP spectra only. (2) Gaia DR3 source id. (3) The fraction of orbits that pass within the specified Galactocentric radius (50 pc and 200 pc) in the last 200 Myr with a large ejection velocity (disc-crossing velocity) of $v_{\text{ej}} > 500 \text{ km s}^{-1}$. (4)-(5) The ejection radius $r_{\text{ej}} = |\mathbf{r}_{\text{ej}}|$ and ejection velocity $v_{\text{ej}} = |\mathbf{v}_{\text{ej}}|$ in the best orbit, respectively. Here, the best orbit is chosen among $N_{\text{MC}} = 10001$ Monte Carlo orbits such that the ejection position is closest to the Galactic center while having a large ejection velocity ($v_{\text{ej}} > 500 \text{ km s}^{-1}$). (6) The flight time since the ejection in the best orbit. (7)-(8) The current Galactocentric spherical radius (r) and cylindrical radius (R) of the star in the best orbit, respectively. (9)-(11) The current velocity of the star in the best orbit. Here, $v = |\mathbf{v}|$ is the magnitude of the current velocity.

Table 4. Chemical properties of our HVS candidates

(1)	(2)	(3)	(4)	(5)	(6)	(7)	(8)	(9)	(10)	(11)
Name	DR3 source_id	[Fe/H] _{spec}	[Mg/Fe] _{spec}	[Si/Fe] _{spec}	[Ca/Fe] _{spec}	[Ti/Fe] _{spec}	[Al/Fe] _{spec}	[α /Fe] _{spec}	[M/H] _{XP}	[α /M] _{XP}
		dex	dex	dex	dex	dex	dex	dex	dex	dex
mrHVSpec1	1364083369852936576	-0.64 ± 0.01	0.35 ± 0.01	0.23 ± 0.02	0.18 ± 0.02	0.12 ± 0.02	0.27 ± 0.02	0.22 ± 0.09	-0.64 ^{+0.18} _{-0.05}	+0.29 ^{+0.09} _{-0.05}
mrHVSpec2	3894254612584073472	-0.81 ± 0.01	0.18 ± 0.02	0.08 ± 0.03	0.18 ± 0.03	0.12 ± 0.04	-0.25 ± 0.03	0.14 ± 0.04	-0.83 ^{+0.14} _{-0.10}	+0.26 ^{+0.05} _{-0.10}
mrHVSpec3	6508950579775204864	-0.50 ± 0.06	0.22 ± 0.02	0.34 ± 0.02	-0.09 ± 0.02	0.02 ± 0.01	-0.43 ± 0.02	0.12 ± 0.17	-0.86 ^{+0.17} _{-0.07}	+0.11 ^{+0.07} _{-0.05}
mrHVSpec4	2694242193191538816	-0.66 ± 0.06	0.39 ± 0.04	0.29 ± 0.03	0.40 ± 0.04	0.28 ± 0.06	0.13 ± 0.11	0.34 ± 0.06	-0.77 ^{+0.27} _{-0.10}	+0.28 ^{+0.03} _{-0.05}
mrHVSpec5	6137389419947219584	-0.83 ± 0.06	0.32 ± 0.03	0.32 ± 0.02	0.24 ± 0.04	0.21 ± 0.02	0.09 ± 0.04	0.27 ± 0.05	-0.97 ^{+0.16} _{-0.14}	+0.07 ^{+0.05} _{-0.05}
mrHVSpec6	5467370673479835904	-0.98 ± 0.07	0.10 ± 0.07	0.30 ± 0.05	0.34 ± 0.06	0.72 ± 0.17	-	0.37 ± 0.22	-1.00 ^{+0.44} _{-0.20}	+0.15 ^{+0.11} _{-0.11}
mrHVSpec7	6692069426721736832	-0.47 ± 0.13	-	-	-	-	0.14 ± 0.13	0.52 ± 0.18	-0.64 ^{+0.11} _{-0.10}	+0.31 ^{+0.04} _{-0.04}
mrHVSpec8	3552388581761193728	-0.90 ± 0.13	-	-	-	-	0.23 ± 0.13	0.39 ± 0.25	-0.95 ^{+0.17} _{-0.16}	+0.22 ^{+0.07} _{-0.08}
mrHVSpec9	3657091157063641344	-0.39	-	-	-	-	-	-	-0.45 ^{+0.09} _{-0.12}	+0.25 ^{+0.05} _{-0.12}
WINERED-HVS1	6434696676903108864	-0.136 ^{+0.040} _{-0.038}	-0.067 ^{+0.075} _{-0.077}	+0.160 ^{+0.081} _{-0.083}	-0.014 ^{+0.169} _{-0.171}	-0.010 ^{+0.122} _{-0.133}	-	0.02 ± 0.09	-0.23 ^{+0.08} _{-0.04}	+0.06 ^{+0.03} _{-0.04}
mrHV Sxp2	4548672495942395264	-	-	-	-	-	-	-	-0.40 ^{+0.11} _{-0.11}	+0.25 ^{+0.03} _{-0.03}
mrHV Sxp3	6173750574418020352	-	-	-	-	-	-	-	-0.56 ^{+0.10} _{-0.12}	+0.15 ^{+0.11} _{-0.04}
mrHV Sxp4	4572287497444895104	-	-	-	-	-	-	-	-0.59 ^{+0.10} _{-0.16}	+0.27 ^{+0.02} _{-0.06}
mrHV Sxp5	6307609625404677376	-	-	-	-	-	-	-	-0.63 ^{+0.16} _{-0.15}	+0.26 ^{+0.04} _{-0.07}
mrHV Sxp6	5765626877690171904	-	-	-	-	-	-	-	-0.69 ^{+0.22} _{-0.22}	+0.25 ^{+0.07} _{-0.07}
mrHV Sxp7	6773393846499438464	-	-	-	-	-	-	-	-0.71 ^{+0.14} _{-0.31}	+0.28 ^{+0.05} _{-0.07}
mrHV Sxp8	6425246443181463680	-	-	-	-	-	-	-	-0.73 ^{+0.17} _{-0.29}	+0.27 ^{+0.04} _{-0.08}
mrHV Sxp9	4501932497166815360	-	-	-	-	-	-	-	-0.84 ^{+0.18} _{-0.25}	+0.07 ^{+0.08} _{-0.03}
mrHV Sxp10	1497611497903517056	-	-	-	-	-	-	-	-0.85 ^{+0.11} _{-0.12}	+0.28 ^{+0.04} _{-0.04}
mrHV Sxp11	1329060763412103808	-	-	-	-	-	-	-	-0.91 ^{+0.19} _{-0.27}	+0.25 ^{+0.05} _{-0.07}
mrHV Sxp12	5130376441238310016	-	-	-	-	-	-	-	-0.93 ^{+0.28} _{-0.17}	+0.27 ^{+0.04} _{-0.07}
mrHV Sxp13	3929723865560075776	-	-	-	-	-	-	-	-0.96 ^{+0.16} _{-0.15}	+0.17 ^{+0.07} _{-0.06}

NOTE— (1) Name of the metal-rich HVS candidates. (2) Gaia DR3 source id. (3)-(9) Chemical abundances from spectroscopic observations. The spectroscopic data for mrHVSpec1-2 are taken from APOGEE DR17 (Abdurro'uf et al. 2022), those for mrHVSpec3-6 are taken from GALAH DR4 (Buder et al. 2024), those for mrHVSpec7-8 are taken from RAVE DR6 (Steinmetz et al. 2020), those for mrHVSpec9 are taken from LAMOST DR9 v2.0 (Zhao et al. 2012), and those for WINERED-HVS1 are derived from our analysis in Section 6. For mrHV Sxp1-6, we adopt $[\alpha/\text{Fe}]_{\text{spec}} = ([\text{Mg}/\text{Fe}]_{\text{spec}} + [\text{Si}/\text{Fe}]_{\text{spec}} + [\text{Ca}/\text{Fe}]_{\text{spec}} + [\text{Ti}/\text{Fe}]_{\text{spec}})/4$ (see also Table 7 for the definition of $[\alpha/\text{Fe}]_{\text{spec}}$). For mrHV Sxp7-8, we adopt $[\alpha/\text{Fe}]_{\text{spec}}$ from RAVE DR6. (10)-(11) The metallicity $[M/H]_{\text{XP}}$ and α -abundance $[\alpha/M]_{\text{XP}}$ estimated from Gaia XP spectra (Hattori 2025).

rest. After thorough examination, we concluded that the systematic bias in the determined line-of-sight velocity, summarized in [Table 5](#), would be $\sim 1.0 \text{ km s}^{-1}$ at most.

With the reduced spectrum, we determined chemical abundances of WINERED-HVS1 with a method similar to those performed by [Kondo et al. \(2019\)](#) and [Fukue et al. \(2021\)](#) using the OCTOMAN code ([Taniguchi et al. 2025](#)), which is a wrapper of the spectral synthesis code MOOG ([Snedden 1973](#); [Snedden et al. 2012](#)). Briefly, we first determined the effective temperature T_{eff} , using the relations between T_{eff} and line-depth ratios (LDRs) of Fe I lines calibrated using well-studied red giants by [Taniguchi et al. \(2021\)](#). Following the procedure described by [Taniguchi et al. \(2025b, in prep.\)](#), we removed the systematic bias in the determined T_{eff} due to the metallicity effect on the T_{eff} -LDR relations. In this step, we adopted the metallicity of WINERED-HVS1 of -0.2624 dex , which is the value tabulated in the Gaia DR3 catalog (`mh_gspphot`) after removing the systematic bias in it following the recipe by [Andrae et al. \(2023b\)](#). The amount of the removed bias is 13 K, which is much smaller than the error in the determined T_{eff} , 76 K. Next, we calculated the surface gravity $\log g$ using the Stefan-Boltzmann law with some stellar parameter values tabulated in the Gaia DR3 catalog: the mass $M = 2.604^{+0.301}_{-0.203} M_{\odot}$, effective temperature $T_{\text{eff}} = 4660.6^{+46.9}_{-58.2} \text{ K}$, and luminosity $L = 51.06^{+8.22}_{-7.52} L_{\odot}$ (`mass_flame`, `teff_gspphot`, and `lum_flame`, respectively). Then, by fitting some of the Fe I lines that are relatively free from the contamination by surrounding lines, we determined v_{micro} and $[\text{Fe}/\text{H}]$ that give no correlation between the line strengths and $[\text{Fe}/\text{H}]$ s determined with the individual lines. Finally, we determined $[\text{X}/\text{H}]$ of Na, Mg, Si, S, K, Ca, Ti, Cr, Ni, and Sr by fitting relatively uncontaminated individual lines of these elements. Throughout the analysis, we used the grid of ATLAS9-APOGEE model atmospheres ([Mészáros et al. 2012](#)). We used two line lists, the list with astrophysical $\log gf$ values calibrated against the Sun by [Meléndez & Barbuy \(1999, MB99\)](#) and the Vienna Atomic Line Database (VALD3; [Ryabchikova et al. 2015](#)), and compared the results to identify potential differences if any.

In determining $[\text{Fe}/\text{H}]$ and $[\text{X}/\text{H}]$, we employed the so-called differential analysis method ([Jofré et al. 2019](#)) to reduce the systematic bias in the determined chemical abundances due to the inaccuracy in infrared line lists (see, e.g., [Andreasen et al. 2016](#); [Matsunaga et al. 2020](#)). As the reference stars of the differential analysis, we analyzed the WINERED spectra of two well-investigated thin-disk red giants, $\varepsilon \text{ Vir}$ and Pollux, observed by [Taniguchi et al. \(2018\)](#). The two stars have the stellar parameters and observed spectra similar to those of WINERED-HVS1. Stellar parameters ($[\text{Fe}/\text{H}]$, T_{eff} , $\log g$, and v_{micro}) and chemical abundances of the two reference stars were mainly adopted from the Gaia FGK benchmark stars v2.1 ([Jofré et al. 2018](#)). They

only determined $[\text{X}/\text{H}]$ of Mg, Si, Ca, Ti, Cr, Fe, and Ni among the elements of our interest, and thus we adopted $[\text{X}/\text{H}]$ of the other elements (Na, S, K, and Sr) from other literature or estimated with an assumption: $[\text{Na}/\text{H}]$ was adopted from the study by [Jofré et al. \(2015\)](#), $[\text{S}/\text{H}]$ and $[\text{K}/\text{H}]$ were estimated assuming $[\text{S}/\text{H}] = [\text{K}/\text{H}] = ([\text{Mg}/\text{H}] + [\text{Si}/\text{H}] + [\text{Ca}/\text{H}])/3$, and $[\text{Sr}/\text{H}]$ was assumed to have the same value as $[\text{Ba}/\text{H}]$ determined by [Jofré et al. \(2015\)](#). Hence, the determined $[\text{X}/\text{H}]$ of Na, S, K, and Sr for WINERED-HVS1 are possibly subject to a systematic bias in the zero point.

Two sources of errors were considered in the analysis: the standard error of line-by-line dispersion and the errors propagated from the errors in stellar parameters (see equations (9) and (10) in [Taniguchi et al. 2025](#)). The errors for most elements are dominated by the standard error of the line-by-line dispersion, but the error propagated from the error in T_{eff} also markedly contribute to some elements (Si, S, Ti, and Cr).

[Fig. 2](#) compares the resultant chemical composition of WINERED-HVS1 determined with the MB99 ([Table 5](#)) and VALD3 ([Table 6](#)) line lists. We found an overall good agreement between the abundances determined with the two lists. Since the MB99 list generally better reproduces near-infrared spectra of late-type stars ([Kondo et al. 2019](#); [Taniguchi et al. 2025](#)), we used the results with the MB99 list, presented in [Table 5](#), in the following discussion. For brevity, we only present $[\text{X}/\text{H}]$ and $[\text{X}/\text{Fe}]$ in [Table 5](#). However, our analysis also allows us to obtain abundance ratio between α elements, such as $[\text{Si}/\text{Mg}] = 0.227^{+0.075}_{-0.075}$, $[\text{Ca}/\text{Mg}] = 0.053^{+0.176}_{-0.178}$, and $[\text{Ti}/\text{Mg}] = 0.058^{+0.150}_{-0.159}$. These $[\text{X}/\text{Mg}]$ ratios will turn out to be informative in understanding the origin of WINERED-HVS1.

7. DISCUSSION

In [Section 5](#), we selected 22 metal-rich HVS candidates from the Gaia DR3 catalog. For one of the candidates, WINERED-HVS1, we conducted high-resolution spectroscopic observations to obtain the detailed chemical abundances (see [Section 6](#)). In this Section, we will first discuss the kinematical ([Table 3](#)) and chemical properties ([Table 4](#)) of these 22 stars. Then we focus on the most-metal rich candidate, WINERED-HVS1, and discuss its origin.

7.1. Kinematical properties of metal-rich HVS candidates

For each metal-rich HVS candidate, we have N_{MC} orbit realizations. By using these Monte Carlo orbits in our fiducial search (i.e., method A in [Table 1](#)), we select the orbits that satisfy either (Condition 1) or (Condition 2), and then find the ‘best’ orbit that has the smallest disc ejection radius r_{ej} . The properties of the best orbit of the metal-rich HVS candidates are summarized in [Table 3](#). In [Fig. 3](#), we show the Monte Carlo orbits as

Table 5. Spectroscopic results of WINERED-HVS1

v_{helio} [km s ⁻¹]	34.79 ± 0.13^a		
T_{eff} [K]	4680 ± 76		
$\log g$	$2.77^{+0.13}_{-0.12}$		
v_{micro} [km s ⁻¹]	$1.559^{+0.139}_{-0.138}$		
[Fe/H] [dex]	$-0.136^{+0.040}_{-0.038}$ (42)		
	[X/H] [dex]	[X/Fe] [dex]	
Na I ^b	$-0.232^{+0.255}_{-0.256}$	$-0.097^{+0.253}_{-0.257}$	(1)
Mg I	$-0.203^{+0.057}_{-0.055}$	$-0.067^{+0.075}_{-0.077}$	(5)
Si I	$+0.024^{+0.068}_{-0.063}$	$+0.160^{+0.081}_{-0.083}$	(16)
Si I ^b	$+0.105^{+0.317}_{-0.305}$	$+0.241^{+0.323}_{-0.317}$	(1)
K I ^b	$+0.339^{+0.264}_{-0.266}$	$+0.475^{+0.263}_{-0.269}$	(1)
Ca I	$-0.150^{+0.167}_{-0.167}$	$-0.014^{+0.169}_{-0.171}$	(5)
Ti I	$-0.145^{+0.135}_{-0.137}$	$-0.010^{+0.122}_{-0.133}$	(10)
Cr I	$-0.190^{+0.138}_{-0.138}$	$-0.054^{+0.133}_{-0.137}$	(7)
Ni I	$-0.143^{+0.179}_{-0.178}$	$-0.008^{+0.179}_{-0.179}$	(2)
Sr II ^b	$-0.272^{+0.272}_{-0.268}$	$-0.137^{+0.274}_{-0.273}$	(1)

NOTE—Chemical abundances, [X/H] and [X/Fe], were determined using the MB99 line list (Meléndez & Barbuy 1999). The results using the VALD3 list are presented in Table 6. Numbers in brackets show the number of lines analyzed.

^aWith a possible systematic bias of ~ 1.0 km s⁻¹ at most.

^b[Na/H], [S/H], [K/H], and [Sr/H] are possibly subject to a systematic bias in the zero point. See text for details.

well as the best orbit for WINERED-HVS1.¹¹ Mainly due to the uncertainty in the heliocentric distance to this star, the ejection location of this star is uncertain, as shown in the left panel of Fig. 3. However, the best orbit (shown in the second panel of Fig. 3) can be traced back to very close to the Galactic center, showing that this star is a candidate of a HVS.

Table 3 indicates that all of the metal-rich HVS candidates have ejection velocities of $v_{\text{ej}} \simeq 500\text{--}600$ km s⁻¹ in their best orbits. This result suggests that they are bound to the Milky Way, because their ejection velocities are lower than the escape velocity near the Galactic center (ignoring the gravity from the SMBH Sgr A*), $v_{\text{esc,GC}} \simeq 700\text{--}800$ km s⁻¹.¹² Indeed, one candidate (mrHVSxp7) is currently moving toward the Galactic center direction (with negative Galactocentric radial ve-

¹¹ We selected this star because we think this is the most promising HVS candidate from chemical analysis. See Section 7.2. Orbits for the other HVS candidates are shown in Figs. 7, 8, 9, 10, and 11, in Appendix D.

¹² We checked some of the widely used Galactic potential models from literature (McMillan 2017; Piffl et al. 2014; Portail et al. 2017). Among these models, the one in Portail et al. (2017) has the smallest value of $v_{\text{esc,GC}} = 684$ km s⁻¹.

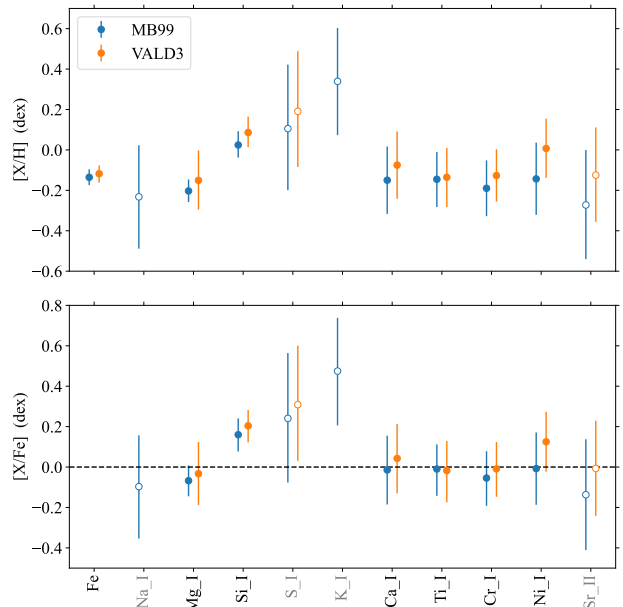


Figure 2. Chemical abundances, [X/H] and [X/Fe], of WINERED-HVS1, summarized in Table 5 (blue; fiducial result using the MB99 line list) and Table 6 (orange; using the VALD3 line list). We employed the differential analysis against two Gaia FGK benchmark stars, ϵ Vir and Pollux. For elements indicated by filled circles, we adopted [X/H] of the reference stars determined by Jofré et al. (2018). In contrast, reference [X/H] of elements indicated by open circles were taken from other literature or estimated with an assumption, and thus they are subject to a possible systematic bias in the zero point. See the main text for more detail.

locity $v_r < 0$; see Fig. 10), which is only possible for a bound HVS.

The only unambiguous HVS known to date is S5-HVS1, whose ejection velocity is estimated to be ~ 1800 km s⁻¹ (Koposov et al. 2020). Compared to the ejection velocity of S5-HVS1, the ejection velocities of our metal-rich HVS candidates are considerably smaller. In terms of the ejection velocity, our sample does not contain unambiguous candidate of HVSs. An independent analysis by Marchetti et al. (2022b) also reached the same conclusion (i.e., they did not find unambiguous HVSs in their analysis). However, we note that the ejection velocities of our metal-rich HVS candidates, $500\text{--}600$ km s⁻¹, are consistent with the theoretical predictions for the ejection velocities of HVSs (Bromley et al. 2006; Brown 2015; Marchetti et al. 2018).

Indeed, in Appendix B, we conducted a Monte Carlo simulation of (bound) HVSs with low ejection velocities with $v_{\text{ej}} \simeq 500\text{--}600$ km s⁻¹. Assuming the stellar mass of $\sim 2M_{\odot}$ (which is a valid assumption for WINERED-HVS1), a typical HVS with $v_{\text{ej}} \simeq 500\text{--}600$ km s⁻¹ has a binary semi-major axis of $a \simeq 2$ AU and the closest ap-

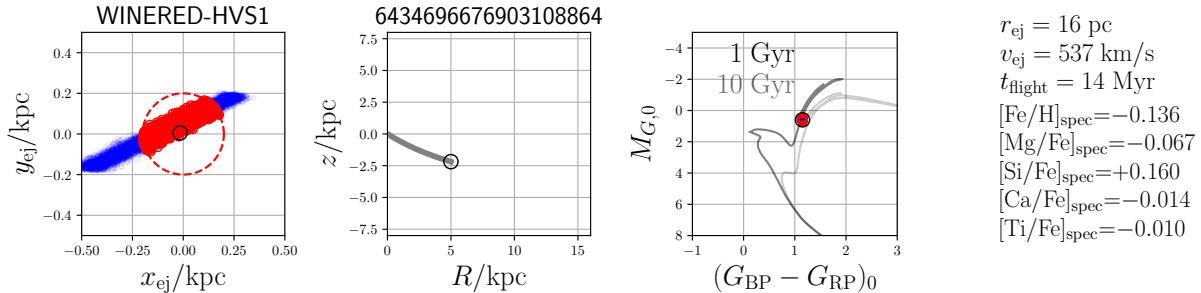


Figure 3. The orbital properties of WINERED-HVS1 (Gaia DR3 6434696676903108864). (Left panel) The ejection locations of the Monte Carlo orbits. The red and blue dots indicate ejections that occurred within and outside $r_{\text{ej}} = 200 \text{ pc}$, respectively. The open black circle indicates the ejection location of the best orbit—the orbit most consistent with an HVS orbit (with the smallest r_{ej}). (Middle panel) The best orbit in the Galactocentric meridional plane. The current location is marked by an open black circle. In the best orbit, WINERED-HVS1 was ejected from the Galactic center 14 Myr ago with an ejection velocity of $v_{\text{ej}} = 537 \text{ km s}^{-1}$. In 5 Myr, the orbit is expected to reach the apocenter at $r = 11.6 \text{ kpc}$. (Right panel) The location of the WINERED-HVS1 in the color-magnitude diagram (CMD). We compute the extinction-corrected color $(G_{\text{BP}} - G_{\text{RP}})_0$ and absolute magnitude $M_{G,0}$ for each Monte Carlo orbit, as different stellar distance is assumed for each orbit. In correcting for the dust extinction, we use a 3D dust map Combined19 from `mwDust` package (Bovy et al. 2016), in which three 3D dust maps are combined (Drimmel et al. 2003; Marshall et al. 2006; Green et al. 2019). The color scheme is the same as in the left panel (e.g., the black open circle corresponds to the location in the CMD for the best orbit). We also plot 1 Gyr and 10 Gyr isochrones from the BaSTI model (Hidalgo et al. 2018), by assuming the stellar metallicity closest to that of this star. The CMD suggests that WINERED-HVS1 is roughly 0.5–10 Gyr old. For a reference, in the right-most part of this figure, we show some physical quantities relevant for this star.

proach to the SMBH of $r_{\text{peri}} \simeq 170 \text{ AU}$ (see Fig. 6). As discussed in Appendix B, the semi-major axis of $a > 1.4 \text{ AU}$ is large enough for two $2-M_{\odot}$ red giants to form a binary system without colliding with each other. Therefore, our HVS candidates may be either (i) ejected as a red giant star; or (ii) ejected as a main-sequence star and evolved into a giant during its flight from the Galactic center to the current position. As shown in Fig. 3, The flight time for the best orbit of WINERED-HVS1 is 14 Myr, which is much shorter than the stellar age of $\sim 0.5\text{--}10 \text{ Gyr}$ estimated from the CMD. Thus, if this star was ejected as a main-sequence star (in the scenario (ii) above), then this star must be ejected at the very final stage of its main-sequence lifetime.

7.2. Chemical properties of metal-rich HVS candidates

Since our HVS candidates are bound to the Milky Way (unlike the unambiguous HVS known as S5-HVS1), the orbital properties alone are not informative enough to constrain the origin of these stars. Rather, given the small ejection rate of HVSs (Brown 2015; see also our discussion in Section 1.2), it would not be surprising if most of our candidates were non-HVSs. In this regard, chemical properties of our candidates, which are summarized in Table 4, are important to understand the origin of these stars.

7.2.1. Metallicity and α -abundance

In the left column of Fig. 4, we compare the metallicity and α -abundance of our HVS candidates with spectroscopic abundances (WINERED-HVS1 and

mrHVSspec1-9) with a sample of reference stars from APOGEE DR17. The top-left and middle-left panels indicate that the APOGEE stars with radial orbits primarily originate from two populations of stars. The first population is the Gaia-Enceladus-Sausage (GES), which is the remnants of the last major merger (Belokurov et al. 2018; Helmi et al. 2018). Because of the near head-on merger of the GES and the ancient Milky Way, the stars originated from GES have nearly radial orbits. The second component is the metal-poor tail of the high- α (disk) stars. This population may be a so-called Splash component, which are the stars in the pre-existing high- α disk that were kicked out of the disk due to the GES merger (Bonaca et al. 2017; Belokurov et al. 2020). These stars may also be kinematically hot tail of the high- α disk stars (see Fig. 15(a)(b) in Hattori 2025). Due to their eccentric orbits, these two populations may contaminate our metal-rich HVS candidates. Most of the radial orbit contaminants have metallicities $[\text{Fe}/\text{H}]_{\text{spec}} < -0.3$. In our selection, we identified 628 APOGEE stars with radial orbits and $[\text{Fe}/\text{H}]_{\text{spec}} > -1$. Notably, among these stars, 626 (99.7%) have $[\text{Fe}/\text{H}]_{\text{spec}} < -0.3$. Our candidates mrHVSspec1-9 exhibit $[\text{Fe}/\text{H}]_{\text{spec}} < -0.3$, similar to the majority of the reference APOGEE sample. Among mrHVSspec1-9, seven of them display high $[\alpha/\text{Fe}]_{\text{spec}} > 0.2$, suggesting they may be metal-poor tail of high- α stars; while two of them show low $[\alpha/\text{Fe}]_{\text{spec}} < 0.2$, indicating that they may belong to the metal-rich tail of the Gaia Enceladus Sausage. (The latter view is supported by the low- $[\text{Al}/\text{Fe}]$ of these two

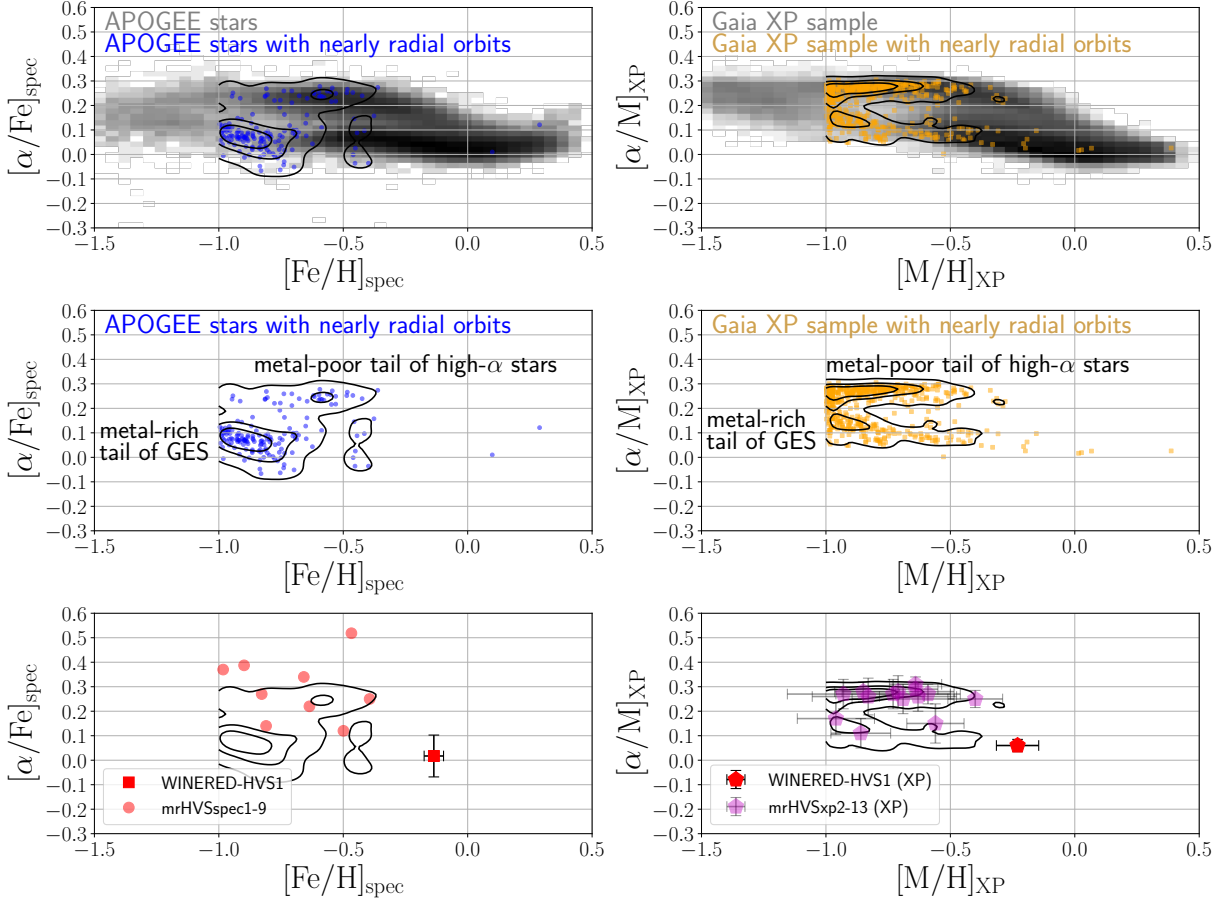


Figure 4. We compare the metallicity and α -abundance of metal-rich stars that exhibit nearly radial orbits (which are presumably non-HVS stars) and those of our HVS candidates. (Left Column) We compare the APOGEE stars and our HVS candidates with known spectroscopic abundances (mrHVSspec1-9 and WINERED-HVS1). The distribution of the cleaned sample of APOGEE DR17 stars is shown by a grayscale image in the top panel. A subset of APOGEE stars with nearly radial orbits and $[\text{Fe}/\text{H}]_{\text{spec}} > -1$ is marked with blue dots, accompanied by contours enclosing 25%, 50%, and 90% of these stars. This group consists of two distinct sequences: the metal-rich tail of Gaia Enceladus Sausage (GES) and the metal-poor tail of high- α disk stars. Notably, 99.7% of stars with nearly radial orbits and $[\text{Fe}/\text{H}]_{\text{spec}} > -1$ satisfy $[\text{Fe}/\text{H}]_{\text{spec}} < -0.3$, and our HVS candidates labeled as mrHVSspec1-9 also meet this criterion. WINERED-HVS1 with $[\text{Fe}/\text{H}]_{\text{spec}} = -0.136$ emerges as the most promising candidate, distinguishing itself as a metal-rich outlier. (Right Column) Next, we compare Gaia XP stars with our XP-based metal-rich HVS candidates (mrHVSxp2-13 and WINERED-HVS1). The top and middle panels are the same as in the left column, but using a cleaned sample of stars with reliable Gaia XP chemistry. About 98% of stars with nearly radial orbits and $[\text{M}/\text{H}]_{\text{XP}} > -1$ have $[\text{M}/\text{H}]_{\text{XP}} < -0.3$, and our HVS candidates labeled as mrHVSxp2-13 also meet this condition. WINERED-HVS1 has a metallicity of $[\text{M}/\text{H}]_{\text{XP}} = -0.23$, which is a clear metal-rich outlier, even when assessed through our XP-based metallicity measurements.

stars, as we will discuss in Section 7.2.2.) These results indicate that our candidates mrHVSspec1-9 are consistent with the majority of non-HVS reference stars, possibly associated with GES (mrHVSspec2-3) or Splash (mrHVSspec1 and mrHVSspec4-9). Among the 628 APOGEE stars, only 2 stars (0.3%) have $[\text{Fe}/\text{H}]_{\text{spec}} > -0.3$,¹³ which indicates that it is very

rare to find a non-HVS with high metallicity and low α -abundance. This result provides a supporting evidence that WINERED-HVS1, which shows an exceptionally high metallicity, is an HVS ejected from the Galactic center. (Indeed, as we will discuss in Section 7.3, the detailed chemical abundances of this star are consistent with the Galactic center population.)

In the right column of Fig. 4, we compare the chemistry of XP-based metal-rich HVS candidates with a sample of (non-HVS) stars with reliable ($[\text{M}/\text{H}]_{\text{XP}}$, $[\alpha/\text{M}]_{\text{XP}}$) estimated from Gaia XP spectra. The

¹³ We have confirmed that these two stars do not exhibit orbits consistent with an HVS.

top-right and middle-right panels confirm the presence of the same two populations of non-HVS stars with nearly radial orbits in the Gaia XP sample.¹⁴ Again, the XP-based metal-rich HVS candidates show $[\text{Fe}/\text{H}]_{\text{spec}} < -0.3$, except for WINERED-HVS1. In terms of the $[\alpha/\text{M}]_{\text{XP}}$ value, mrHVSxp3,9,13 may be possibly associated with the GES component, while mrHVSxp2,4-8,10-12 may be possibly associated with the Splash component.

Based on the distribution of stars in $([\text{Fe}/\text{H}]_{\text{spec}}, [\alpha/\text{Fe}]_{\text{spec}})$ -space or $([\text{M}/\text{H}]_{\text{XP}}, [\alpha/\text{M}]_{\text{XP}})$ -space, we conclude that

- WINERED-HVS1 is the most promising candidate for an HVS ejected from the Galactic center (see also [Section 7.3](#)).

Compared to WINERED-HVS1, the other metal-rich HVS candidates (mrHVSspec1-9 and mrHVSxp2-13) are less attractive, but we do not have strong evidence to conclude that they are non-HVSs. However, if we assume—as a working hypothesis—that they are non-HVSs, then our best guess for their origins are as follows:

- mrHVSspec2-3 (see also [Section 7.2.2](#)) and mrHVSxp3,9,13 are possibly metal-rich tail of GES stars;
- mrHVSspec1,4-9 and mrHVSxp2,4-8,10-12 are possibly metal-poor tail of Splash stars;

Under this working hypothesis, we only find one HVS (candidate) from our Gaia DR3 catalog with Gaia XP spectra. The statistical implication of this result is discussed in [Appendix C](#).

7.2.2. $[\text{Al}/\text{Fe}]$ -abundance

In understanding the origin of HVS candidates, the abundance ratio of $[\text{Al}/\text{Fe}]$ is also informative. As we discussed earlier, one of the sources of contamination to the HVSs is the GES, which dominates the stellar halo within 20 kpc from the Galactic center. A distinct feature of GES stars is that they typically show negative $[\text{Al}/\text{Fe}]$ ([Feuillet et al. 2021](#)), unlike other Milky Way

¹⁴ In the reference APOGEE sample (blue dots in the middle-left panel in [Fig. 4](#)), we see more GES-like stars than Splash-like stars. In contrast, in the reference Gaia XP sample (orange dots in the middle-right panel in [Fig. 4](#)), we see more Splash-like stars than GES-like stars. We do not fully understand the origin for this difference, but it may be due to the sample selection effect, such that we see low Galactic latitude region for the APOGEE sample and we see high Galactic latitude region (with low dust extinction; [Hattori 2025](#)) for the Gaia XP sample. In this regard, it is interesting to point out that our candidates mrHVSspec1-9 and mrHVSxp2-13 are selected from the catalog of [Hattori \(2025\)](#), and we see more Splash-like HVS candidates than GES-like HVS candidates, similar to the distribution of orange dots in the middle-right panel in [Fig. 4](#).

stars such as thin disk, thick disk, or bulge stars ([Das et al. 2020](#); [Feuillet et al. 2022](#); [Barbuy et al. 2023](#); [Nandakumar et al. 2024](#)). Therefore, the $[\text{Al}/\text{Fe}]$ ratio is informative to flag possible GES stars.

Among 22 HVS candidates, we have $[\text{Al}/\text{Fe}]$ measurements for 7 stars, and two stars (mrHVSspec2 and mrHVSspec3) have $[\text{Al}/\text{Fe}] \lesssim -0.2$ (as shown in [Table 4](#)). The $[\text{Al}/\text{Fe}]$ values of these stars indicate that mrHVSspec2 and mrHVSspec3 are consistent with GES stars.¹⁵ Intriguingly, these two stars have $[\alpha/\text{Fe}]_{\text{spec}} = 0.14$ and 0.12 , respectively, and have the lowest $[\alpha/\text{Fe}]_{\text{spec}}$ among mrHVSspec1-9. In the $([\text{Fe}/\text{H}]_{\text{spec}}, [\alpha/\text{Fe}]_{\text{spec}})$ -space, these stars lie almost along the sequence of the metal-rich tail of the GES stars (see the lower-left panel of [Fig. 4](#)). Both $[\text{Al}/\text{Fe}]$ and $[\alpha/\text{Fe}]_{\text{spec}}$ indicate that mrHVSspec2 and mrHVSspec3 are consistent with GES stars. However, we stress that this argument needs to be handled with care, because currently we do not know the $[\text{Al}/\text{Fe}]$ ratio for any stars in the Galactic center. For example, if future observations indicate that Galactic center stars show low- $[\text{Al}/\text{Fe}]$, each of mrHVSspec2 and mrHVSspec3 can be considered a good candidate for either an HVS or a GES star.

7.3. Chemistry of WINERED-HVS1 compared to other stars in the Milky Way and beyond

Now we focus on the most metal-rich candidate, WINERED-HVS1. To gain some insights into its origin, we will compare the chemistry of this star with that of stars in the NSC, NSD, inner bulge, and dwarf galaxies. Throughout this section, we utilize $[\text{X}/\text{Y}]$ instead of $[\text{X}/\text{Y}]_{\text{spec}}$ for brevity, since we only deal with spectroscopically determined chemical abundances.

(1) Nuclear Star Cluster (NSC)

The SMBH at the center of the Milky Way is surrounded by a dense and massive star cluster known as the NSC, whose radius is estimated to be $\simeq 4$ pc ([Schödel et al. 2014](#)). According to the Hills mechanism ([Hills 1988](#)), when the SMBH disrupts a binary star system at a typical radius of ~ 100 AU $\simeq 5 \times 10^{-4}$ pc, it ejects one star as an HVS while capturing the companion star as an S-star. Since HVS ejections happen at the central part of the NSC, we expect a chemical similarity between the HVSs and the NSC stars.

The observed chemical abundances for NSC stars (including an S-star) are summarized in the left column of [Fig. 5](#). As seen from the metallicity distribution of the NSC stars (bottom panel; [Feldmeier-Krause et al. 2020](#); [Do et al. 2015](#); see also [Rich et al. 2017](#)), the majority of stars in the NSC have super-solar metallicity, while more than $\sim 10\%$ of the stars show sub-solar metallicity. The

¹⁵ Since we do not know the $[\text{Al}/\text{Fe}]$ of stars in the immediate neighbor of the SMBH, low- $[\text{Al}/\text{Fe}]$ nature of these stars does not necessarily mean that they are non-HVSs. However, their low- $[\text{Al}/\text{Fe}]$ nature does flag that they may be GES stars.

observed metallicity of $[\text{Fe}/\text{H}] = -0.136$ for WINERED-HVS1 is within the metallicity range of NSC stars. Also, the values of $[\alpha/\text{Fe}]$, $[\text{Mg}/\text{Fe}]$, $[\text{Si}/\text{Mg}]$, and $[\text{Ca}/\text{Mg}]$ for WINERED-HVS1 are within the range of the nine NSC red giants at 0.3–4 pc from the SMBH analyzed by Ryde et al. (2025) (black open diamonds). Therefore, broadly speaking, the chemistry of WINERED-HVS1 is consistent with that of NSC stars. Of course, a more detailed comparison with larger number of NSC stars is required to support this view. For example, the nine red giant stars analyzed by Ryde et al. (2025) include two stars with solar or slightly sub-solar $[\text{Fe}/\text{H}]$. Although these two stars have similar metallicity to WINERED-HVS1, they have slightly higher $[\text{Mg}/\text{Fe}]$ and slightly lower $[\text{Si}/\text{Mg}]$ than WINERED-HVS1. It is unclear if these differences are serious or benign, especially because (i) we have only two NSC stars to make a comparison; (ii) $[\text{Mg}/\text{Fe}]$ and $[\text{Si}/\text{Mg}]$ for the NSC stars and WINERED-HVS1 are associated with non-negligible uncertainties (~ 0.1 dex); and (iii) these two stars and WINERED-HVS1 are observed and analyzed in a different manner, and hence subject to a possible systematic bias in the zero point.

The blue upside-down triangle in the left column of Fig. 5 shows the chemistry of S0-6/S10. This star is the only S-star for which detailed chemistry is known (Nishiyama et al. 2024), and it is located only 0.012 pc away from the SMBH. The chemistry of the nine NSC stars in Ryde et al. (2025) is not particularly similar to that of S0-6/S10, although these nine red giants, along with the S0-6/S10, are all located within the NSC. This difference might indicate the chemical inhomogeneity within the NSC (Feldmeier-Krause et al. 2020). Intriguingly, in the $([\text{Fe}/\text{H}], [\text{Mg}/\text{Fe}])$ -space, WINERED-HVS1 is located in between the S0-6/S10 and the sample in Ryde et al. (2025). Since we only have one S-star and one HVS candidate, we can not draw a useful conclusion as to whether the HVSs and S-stars have similar chemical properties as a population.

(2) Nuclear Stellar Disk (NSD)

NSD is a rotationally supported stellar disk at the central part of the Milky Way. It extends to ~ 220 pc in radius with a scale height of ~ 50 pc (Nishiyama et al. 2013; Schultheis et al. 2021). Feldmeier-Krause (2022) studied the chemical abundances of stars within the NSD to find that NSC and NSD show different chemistry, such that NSD stars are typically more metal-poor than NSC stars.

The chemical properties of NSD is summarized in the second column in Fig. 5. The black filled circles show the NSD stars analyzed by Ryde et al. (2016b). The open gray circles show the NSD stars in APOGEE selected by Schultheis et al. (2020). In the original study of Schultheis et al. (2020), they used the chemical abundances in APOGEE DR16, while in this figure we adopt the more recent values from APOGEE DR17. The cyan circle is a metal-poor NSD star known as

GC10812,¹⁶ whose metallicity almost corresponds to the lowest metallicity of the NSD sample in Schultheis et al. (2020). The two NSD samples from Ryde et al. (2025) and Schultheis et al. (2020) show a broadly consistent profiles of $[\alpha/\text{Fe}]$, $[\text{Mg}/\text{Fe}]$ and $[\text{Si}/\text{Mg}]$ as a function of $[\text{Fe}/\text{H}]$. Notably, the value of $[\text{Si}/\text{Mg}]$ for the sample in Schultheis et al. (2020) is almost insensitive to $[\text{Fe}/\text{H}]$. This trend is also true for the sample of Ryde et al. (2016b), although we see a larger scatter for this sample. Interestingly, the low- $[\text{Si}/\text{Mg}]$ nature of the NSD stars seems to be inconsistent with the high $[\text{Si}/\text{Mg}]$ ratio observed for WINERED-HVS1. Also, the observed $[\text{Mg}/\text{Fe}]$ ratio of WINERED-HVS1 is slightly smaller than $[\text{Mg}/\text{Fe}]$ of both Ryde et al. (2016b) sample and Schultheis et al. (2020) sample. The offset in $[\text{Si}/\text{Mg}]$ (and a marginal offset in $[\text{Mg}/\text{Fe}]$) may indicate that the WINERED-HVS1 is not chemically consistent with the stellar population in the NSD.

(3) Inner bulge

We further investigate the chemical properties of the inner bulge (within ~ 300 pc or ~ 2 degrees from the Galactic center), which are summarized in the third column of Fig. 5. Here, the black plus and orange cross correspond to the inner bulge samples taken from Nandakumar et al. (2024) and Ryde et al. (2016b), respectively. Most notably, the inner bulge stars show low values of $[\text{Si}/\text{Mg}]$, which is in contrast to the high- $[\text{Si}/\text{Mg}]$ ratio seen in WINERED-HVS1. This discrepancy indicates that the WINERED-HVS1 is chemically distinct from inner bulge stars.

(4) Dwarf galaxies

The $[\text{Fe}/\text{H}]$ and $[\alpha/\text{Fe}]$ of WINERED-HVS1 resembles that of stars found at the metal-rich end of massive dwarf galaxies. Motivated by this fact, we compare WINERED-HVS1 with stars in dwarf galaxies and GES (remnants of a disrupted dwarf galaxy). In the right-most column in Fig. 5, we summarize the chemical properties of stars in the LMC (pink ‘L’; Van der Swaelmen et al. 2013), Sagittarius dwarf galaxy (purple ‘S’; Minelli et al. 2021), and the GES (green ‘G’; APOGEE DR17 data with a selection similar to that in Feuillet et al. 2021).

The stars in the GES are not as metal-rich as WINERED-HVS1, which may be due to the quenched star formation in the GES when it merged to the Milky Way (Ernandes et al. 2024). The mismatch between the chemistry of GES stars and that of WINERED-HVS1 supports our view that WINERED-HVS1 is not associated with the GES.

The other massive, surviving dwarf galaxies in this plot (LMC and Sagittarius) are large enough to maintain star formation activity for a long duration of time.

¹⁶ The projected distance of this star from the SMBH is 1.5 pc, but Ryde et al. (2016a) and Ryde et al. (2025) interpret this star as a NSD star, based on its kinematics and photometric information.

Therefore, some stars located in the central part of the LMC and Sagittarius dwarf galaxy are as metal-rich as WINERED-HVS1. For example, the Sagittarius dwarf galaxy has a NSC known as M54 (Alfaro-Cuello et al. 2019), in which young (~ 1 Gyr old) and metal-rich stars are confirmed. Although WINERED-HVS1 is metal-rich, it is unclear if this star is as young as ~ 1 Gyr old. (Our current guess of its age is 0.5–10 Gyr based on the CMD in Fig. 3 and quite uncertain.) However, if WINERED-HVS1 is indeed young, we see a similarity between WINERED-HVS1 and the metal-rich stars in massive dwarf galaxies. In such a case, WINERED-HVS1 might have formed in the NSC of a massive dwarf galaxy. If this star was formed in the NSC of a massive dwarf galaxy, and yet it was ejected from the Galactic center, we need to speculate a scenario to bring this star from its progenitor dwarf galaxy to the Galactic center.

It is unrealistic to suggest that this star was formed in the Sagittarius (or LMC) and was later brought to the Milky Way’s NSC because the apocenter distance of this star is too small to have originated from these surviving dwarf galaxies. Therefore, it is more likely that WINERED-HVS1 was formed in the NSC of a hypothetical massive dwarf galaxy that later merged with the Milky Way. If this hypothetical dwarf galaxy was massive enough to host an NSC, the dynamical friction might have brought the dwarf galaxy and its NSC to the Galactic center. Then the dwarf galaxy’s NSC can merge with the Milky Way’s NSC.¹⁷

If WINERED-HVS1 was formed before the NSC merger, it could reflect the chemistry of the dwarf galaxy’s NSC. Also, if WINERED-HVS1 was brought to the center of the Milky Way’s NSC, it could be ejected as a Galactic HVS. Indeed, the Milky Way’s NSC exhibits an asymmetric spatial distribution of sub-solar metallicity stars (Feldmeier-Krause et al. 2020), which can be interpreted as a result of the merger of NSCs within the last ~ 3 Gyr—a time frame recent enough to retain the dynamical relics (Arca Sedda et al. 2020).

There are several caveats to our scenario. If the merger with this hypothetical dwarf galaxy occurred recently and if that dwarf galaxy was sufficiently massive to host an NSC, we should expect to see the stellar stream of its merger debris in the halo. Thus, the merger must have happened a long time ago (~ 10 Gyr). In this context, a hypothetical dwarf galaxy known as Kraken

(also known as Heracles), which is a dwarf galaxy with a stellar mass of $\sim 10^9 M_\odot$ claimed to contribute to the central part of the Milky Way (Kruijssen et al. 2019; Horta et al. 2021), might be a good candidate for the progenitor dwarf galaxy of WINERED-HVS1. Although the Kraken dwarf galaxy is predominantly composed of metal-poor and high- α stars ($[\text{Fe}/\text{H}] \simeq -1$ and $[\text{Mg}/\text{Fe}] \simeq 0.3$; Horta et al. 2023), its NSC could be as metal-rich and low- α as WINERED-HVS1.

Assuming the progenitor dwarf galaxy (possibly Kraken) merged with the Milky Way ~ 10 Gyr ago, we need to explore a mechanism that would gradually bring its NSC to the Galactic center over a timescale of ~ 7 Gyr (if we presume the NSC merger occurred 3 Gyr ago). According to the simulations in Arca Sedda et al. (2020), some models classified as ‘late infalls’ satisfy this condition. Therefore, while not entirely convincing, it may be possible for WINERED-HVS1 to have formed in the NSC of a massive dwarf galaxy and been ejected from the Galactic center.

More detailed chemical abundances of WINERED-HVS1, such as its abundances of r -process elements, are required to fully understand the birth environment of this star.¹⁸

7.4. Future prospect

In the future, we plan to extend this work to better characterize the metal-rich HVSs.

7.4.1. Use of other large catalogs

In this work, we used the catalog of 48 million stars published by Hattori (2025) to search for metal-rich HVSs. We selected this catalog because it is the largest catalog in which both metallicity and α -abundance are available. In the hindsight, however, the metallicity information is more important than α -abundance information in identifying HVS candidates. Thus, it may be beneficial to utilize existing large catalogs of metallicity, such as those by Andrae et al. 2023a and Zhang et al. 2023, which provide metallicity data for 175 million and 220 million stars, respectively. This approach could help in identifying metal-rich HVS candidates, even if the catalogs do not include α -abundance information.

Several ongoing or upcoming stellar surveys, including but not limited to WEAVE (Jim et al. 2023), 4MOST (de Jong et al. 2019), and PFS (Takada et al. 2014),

¹⁷ If this scenario holds true, it is possible to propose an alternative scenario in which WINERED-HVS1 was formed in a Young Massive Cluster (Portegies Zwart et al. 2010) within the stellar disk. If the progenitor cluster was later dragged to the Galactic center due to the dynamical friction and merged to the NSC, WINERED-HVS1 could be ejected by the SMBH. However, this scenario cannot account for the origin of WINERED-HVS1, as stars in Young Massive Clusters typically exhibit chemistry similar to that of low- α disk stars, which is characterized by a low value of $[\text{Si}/\text{Mg}]$ and inconsistent with the high value of $[\text{Si}/\text{Mg}] = 0.227^{+0.075}_{-0.075}$ for this star.

¹⁸ In this context, it is important to mention the work by Nishiyama et al. (2024). According to their study, the S-star known as S0-6/S10 is more than 10 Gyr old and its $[\text{Fe}/\text{H}]$ and $[\alpha/\text{Fe}]$ are similar to some metal-rich stars in massive dwarf galaxies such as LMC and Sagittarius. We note that metal-rich stars in massive dwarf galaxies have a relatively young age (~ 1 Gyr old), and therefore stars like S0-6/S10, namely old and metal-rich stars, cannot be formed in large dwarf galaxies. For our HVS candidate WINERED-HVS1, the stellar age is around 0.5–10 Gyr. Thus, in case it is young (~ 1 Gyr old), this star could be more or less similar to the metal-rich stars in massive dwarf galaxies.

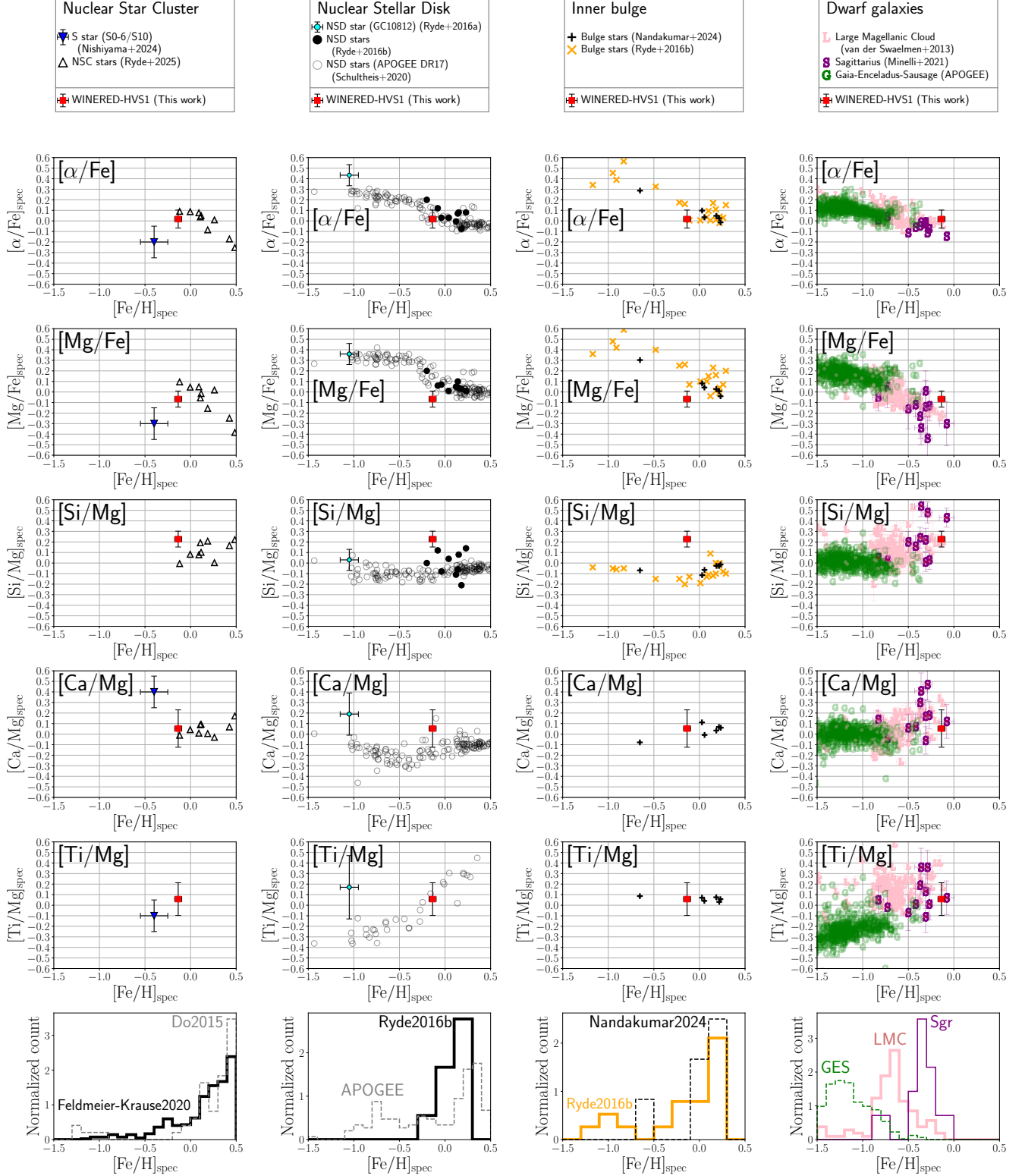


Figure 5. Chemistry of WINERED-HVS1 compared with stars in the NSC (left column), NSD (second column), inner bulge (third column), and dwarf galaxies (fourth column). The metal-rich, low- $[\text{Mg}/\text{Fe}]$ and high- $[\text{Si}/\text{Mg}]$ nature of WINERED-HVS1 is most consistent with the NSC stars. Intriguingly, WINERED-HVS1 is chemically similar to the metal-rich stars in massive dwarf galaxies; and it might have formed in the core of massive dwarf galaxy that merged to the Milky Way.

are measuring the line-of-sight velocities for millions of stars. For many of these stars, this will be the first time their line-of-sight velocities have been measured. These new catalogs, when combined with the astrometric data from Gaia, will allow us identify more HVS candidates.

7.4.2. Longer integration time

In this paper, we focused on recently ejected HVS candidates, because the orbital uncertainties would increase if we were to integrate the orbit backward for a longer time. Nonetheless, it could be interesting to search for other bound HVSs which have been ejected more than ~ 200 Myr ago, as bound HVSs are not necessarily recently ejected.

7.4.3. Optical view of the Galactic center environment using hyper-velocity stars

In [Section 6](#), we use the near-infrared YJ -band spectrum to derive the chemical abundances of WINERED-HVS1. As this star is moving in the halo region (see [Fig. 3](#)), where dust extinction is minimal, we can obtain an optical spectrum for this star. The optical spectrum contains absorption lines of several heavy elements (such as Eu and other r -process elements) that are not available in an infrared spectrum with measurable strengths. By analyzing the chemical abundances of WINERED-HVS1 from its optical spectrum, we may gain insights into the chemical landscape near the Galactic center.

Traditionally, understanding the Galactic center environment has been challenging due to the high levels of dust in that direction, which demands extensive telescope time, especially in the near-infrared K band. By searching for many more HVSs and by characterizing their chemical abundances with optical spectra, we will open a new window into the Galactic center environment without being hindered by dust obscuration.

8. SUMMARY AND CONCLUSION

By using astrometric data from Gaia DR3, photometric distance from StarHorse catalog ([Anders et al. 2022](#)), and metallicity along with α -abundance derived from the Gaia XP spectra from the catalog of [Hattori \(2025\)](#), we searched for candidates of metal-rich HVSs that were ejected recently (in the last ~ 200 Myr) from the Galactic center and we only consider HVS candidates that have experienced no disk crossings after the ejection. Our assumptions limit our search to either (a) unbound HVSs or (b) bound HVSs that have not experienced disk crossing after ejection. After selecting stars with some quality cut and a rough metallicity cut ($[M/H]_{XP} > -1$), we searched for stars that are kinematically consistent with HVSs ejected from the Galactic center. We conducted the HVS search by using four different sets of assumptions on the gravitational potential of the Milky Way and on the Solar position/velocity (see [Table 1](#)). As a result, we find 74 kinematically selected metal-rich

HVS candidates that are robust against the different assumptions on the Milky Way potential and Solar position/velocity. All of these HVS candidates are bound to the Milky Way.

We further pruned the sample by using the chemical information to identify 22 metal-rich HVS candidates, all of which turned out to be red giant stars (see [Fig. 1](#)). Unlike the only unambiguous HVS candidate, S5-HVS1 ([Koposov et al. 2020](#)), all our candidates are gravitationally bound to the Milky Way, and their ejection velocities are $500\text{--}600$ km s $^{-1}$ (see [Table 3](#)). Thus, chemical characterizations of these stars is essential for understanding their origins.

Among these 22 candidates, 9 HVS candidates (labeled as mrHVSspec1-9) have spectroscopic abundances derived from large surveys (APOGEE, GALAH, RAVE, and LAMOST; see [Table 4](#)). The remaining 13 HVS candidates (labeled as WINERED-HVS1 and mrHVSxp2-13) lack existing spectroscopic abundances, but have relatively reliable estimates of ($[M/H]_{XP}$, $[\alpha/M]_{XP}$) from Gaia XP spectra ([Hattori 2025](#)) (see [Table 4](#)).

Based on the metallicity and α -abundance of these stars, we cannot ignore the possibility that 21 stars out of our 22 candidates may be non-HVSs. Namely, these 21 stars might be part of either the metal-rich tail of the GES (which is the remnants of the ancient major merger; [Helmi et al. 2018](#); [Belokurov et al. 2018](#)), or the metal-poor tail of the high- α disk (which may be so-called Splash stars kicked out of the pre-existing disk when GES merged to the ancient Milky Way; [Bonaca et al. 2017](#); [Belokurov et al. 2020](#)). In contrast to these 21 stars, one candidate, WINERED-HVS1, has a near-solar value of $[M/H]_{XP}$, making it unlikely to be classified as either a GES star or a Splash star.

To investigate this star further, we conducted a follow-up observation with Magellan/WINERED (see [Section 6](#)). Through a careful analysis of its high-resolution spectrum in the near-infrared YJ bands, we determined the metallicity $[Fe/H]$ as well as the abundances for Na, Mg, Si, S, K, Ca, Ti, Cr, Ni, and Sr (see [Table 5](#)). We obtained the metallicity and α -abundance ($[Fe/H] = -0.136^{+0.040}_{-0.038}$, $[Mg/Fe] = -0.067^{+0.075}_{-0.077}$), which are consistent with the Gaia-XP-based chemical abundances.

To better understand the origin of this star, we compared the chemical properties of WINERED-HVS1 with those of other stars in the Milky Way and beyond (see [Fig. 5](#)). We found that WINERED-HVS1 is chemically consistent with stars in the NSC, but somewhat inconsistent with stars in the NSD or inner bulge, mainly due to its high $[Si/Mg]$ ratio. This result is promising, as HVSs are ejected from the central region of the NSC, where the SMBH resides. Though the metallicity of WINERED-HVS1 is lower than that of typical NSC stars, it remains consistent with the metal-poor tail of NSC stars.

Another interesting point regarding the chemistry of WINERED-HVS1 is that the chemical abundance pat-

tern of WINERED-HVS1 resembles the abundance pattern of the metal-rich stars in massive dwarf galaxies, such as the LMC or the Sagittarius dwarf galaxy. We do not think that WINERED-HVS1 was formed in either of these dwarf galaxies, because bringing this star to the central part of the Milky Way is unrealistic from a dynamical point of view. However, this chemical similarity indicates that this star may have formed in an environment similar to the core of a more massive dwarf galaxy. Further observational studies are awaited to better understand the birth environment of this star.

K.H. thanks Sergey E. Koposov for the inspiring collaboration at CMU, which provided valuable insights. Some of the insights gained during that time form a foundation for this work. K.H. is supported by JSPS KAKENHI Grant Numbers JP24K07101, JP21K13965, and JP21H00053. D.T. acknowledges financial support by the JSPS Research Fellowship for Young Scientists and the accompanying JSPS KAKENHI Grant Number 23KJ2149. T.T. acknowledges the support by JSPS KAKENHI Grant No. 23H00132.

This paper uses the WINERED data gathered with the 6.5 meter Magellan Telescope located at Las Campanas Observatory, Chile. We are grateful to Yuki Sarugaku, Tomomi Takeuchi, and the staff of Las Campanas Observatory for their support during the WINERED's observations. WINERED was developed by the Uni-

versity of Tokyo and the Laboratory of Infrared High-resolution Spectroscopy, Kyoto Sangyo University, under the financial support of KAKENHI (Nos. 16684001, 20340042, and 21840052) and the MEXT Supported Program for the Strategic Research Foundation at Private Universities (Nos. S0801061 and S1411028). The observing run in 2023 June was partly supported by KAKENHI (grant No. 19KK0080) and JSPS Bilateral Program Number JPJSBP120239909.

This work has made use of data from the European Space Agency (ESA) mission *Gaia* (<https://www.cosmos.esa.int/gaia>), processed by the *Gaia* Data Processing and Analysis Consortium (DPAC, <https://www.cosmos.esa.int/web/gaia/dpac/consortium>). Funding for the DPAC has been provided by national institutions, in particular the institutions participating in the *Gaia* Multilateral Agreement.

Facility: Magellan/WINERED, Gaia

Software: Agama (Vasiliev 2019), ATLAS9-APOGEE (Mészáros et al. 2012), BaSTI (Pietrinferni et al. 2004; Hidalgo et al. 2018), MOOG (Snedden 1973; Sneden et al. 2012), *mwDust* (Bovy et al. 2016), OCTOMAN (Taniguchi et al. 2025), SAGA (Suda et al. 2008), WARP (Hamano et al. 2024), matplotlib (Hunter 2007), numpy (van der Walt et al. 2011), scipy (Virtanen et al. 2020)

REFERENCES

- Abdurro'uf, Accetta, K., Aerts, C., et al. 2022, *ApJS*, 259, 35, doi: [10.3847/1538-4365/ac4414](https://doi.org/10.3847/1538-4365/ac4414)
- Akiba, T., Naoz, S., & Madigan, A.-M. 2024, arXiv e-prints, arXiv:2410.19881, doi: [10.48550/arXiv.2410.19881](https://doi.org/10.48550/arXiv.2410.19881)
- Alfaro-Cuello, M., Kacharov, N., Neumayer, N., et al. 2019, *ApJ*, 886, 57, doi: [10.3847/1538-4357/ab1b2c](https://doi.org/10.3847/1538-4357/ab1b2c)
- Anders, F., Khalatyan, A., Queiroz, A. B. A., et al. 2022, *A&A*, 658, A91, doi: [10.1051/0004-6361/202142369](https://doi.org/10.1051/0004-6361/202142369)
- Andrae, R., Rix, H.-W., & Chandra, V. 2023a, *ApJS*, 267, 8, doi: [10.3847/1538-4365/acd53e](https://doi.org/10.3847/1538-4365/acd53e)
- Andrae, R., Fouesneau, M., Sordo, R., et al. 2023b, *A&A*, 674, A27, doi: [10.1051/0004-6361/202243462](https://doi.org/10.1051/0004-6361/202243462)
- Andreasen, D. T., Sousa, S. G., Delgado Mena, E., et al. 2016, *A&A*, 585, A143, doi: [10.1051/0004-6361/201527308](https://doi.org/10.1051/0004-6361/201527308)
- Arca Sedda, M., Gualandris, A., Do, T., et al. 2020, *ApJL*, 901, L29, doi: [10.3847/2041-8213/abb245](https://doi.org/10.3847/2041-8213/abb245)
- Barbuy, B., Friaça, A. C. S., Ernandes, H., et al. 2023, *MNRAS*, 526, 2365, doi: [10.1093/mnras/stad2888](https://doi.org/10.1093/mnras/stad2888)
- Belokurov, V., Erkal, D., Evans, N. W., Koposov, S. E., & Deason, A. J. 2018, *MNRAS*, 478, 611, doi: [10.1093/mnras/sty982](https://doi.org/10.1093/mnras/sty982)
- Belokurov, V., Sanders, J. L., Fattahi, A., et al. 2020, *MNRAS*, 494, 3880, doi: [10.1093/mnras/staa876](https://doi.org/10.1093/mnras/staa876)
- Bennett, M., & Bovy, J. 2019, *MNRAS*, 482, 1417, doi: [10.1093/mnras/sty2813](https://doi.org/10.1093/mnras/sty2813)
- Bland-Hawthorn, J., & Gerhard, O. 2016, *ARA&A*, 54, 529, doi: [10.1146/annurev-astro-081915-023441](https://doi.org/10.1146/annurev-astro-081915-023441)
- Bonaca, A., Conroy, C., Wetzell, A., Hopkins, P. F., & Kereš, D. 2017, *ApJ*, 845, 101, doi: [10.3847/1538-4357/aa7d0c](https://doi.org/10.3847/1538-4357/aa7d0c)
- Bovy, J., Rix, H.-W., Green, G. M., Schlafly, E. F., & Finkbeiner, D. P. 2016, *ApJ*, 818, 130, doi: [10.3847/0004-637X/818/2/130](https://doi.org/10.3847/0004-637X/818/2/130)
- Bressan, A., Marigo, P., Girardi, L., et al. 2012, *MNRAS*, 427, 127, doi: [10.1111/j.1365-2966.2012.21948.x](https://doi.org/10.1111/j.1365-2966.2012.21948.x)
- Bromley, B. C., Kenyon, S. J., Geller, M. J., et al. 2006, *ApJ*, 653, 1194, doi: [10.1086/508419](https://doi.org/10.1086/508419)
- Brown, W. R. 2015, *ARA&A*, 53, 15, doi: [10.1146/annurev-astro-082214-122230](https://doi.org/10.1146/annurev-astro-082214-122230)
- Brown, W. R., Geller, M. J., Kenyon, S. J., & Kurtz, M. J. 2005, *ApJL*, 622, L33, doi: [10.1086/429378](https://doi.org/10.1086/429378)
- Buder, S., Kos, J., Wang, E. X., et al. 2024, arXiv e-prints, arXiv:2409.19858, doi: [10.48550/arXiv.2409.19858](https://doi.org/10.48550/arXiv.2409.19858)

- Carr, J. S., Sellgren, K., & Balachandran, S. C. 2000, *ApJ*, 530, 307, doi: [10.1086/308340](https://doi.org/10.1086/308340)
- Clementini, G., Ripepi, V., Garofalo, A., et al. 2023, *A&A*, 674, A18, doi: [10.1051/0004-6361/202243964](https://doi.org/10.1051/0004-6361/202243964)
- Cunha, K., Sellgren, K., Smith, V. V., et al. 2007, *ApJ*, 669, 1011, doi: [10.1086/521813](https://doi.org/10.1086/521813)
- Cutri, R. M., Skrutskie, M. F., van Dyk, S., et al. 2003, 2MASS All Sky Catalog of point sources.
- Das, P., Hawkins, K., & Jofré, P. 2020, *MNRAS*, 493, 5195, doi: [10.1093/mnras/stz3537](https://doi.org/10.1093/mnras/stz3537)
- Davies, B., Origlia, L., Kudritzki, R.-P., et al. 2009, *ApJ*, 694, 46, doi: [10.1088/0004-637X/694/1/46](https://doi.org/10.1088/0004-637X/694/1/46)
- De Angeli, F., Weiler, M., Montegriffo, P., et al. 2023, *A&A*, 674, A2, doi: [10.1051/0004-6361/202243680](https://doi.org/10.1051/0004-6361/202243680)
- de Jong, R. S., Agertz, O., Berbel, A. A., et al. 2019, *The Messenger*, 175, 3, doi: [10.18727/0722-6691/5117](https://doi.org/10.18727/0722-6691/5117)
- Deason, A. J., Belokurov, V., & Sanders, J. L. 2019, *MNRAS*, 490, 3426, doi: [10.1093/mnras/stz2793](https://doi.org/10.1093/mnras/stz2793)
- Do, T., Kerzendorf, W., Winsor, N., et al. 2015, *ApJ*, 809, 143, doi: [10.1088/0004-637X/809/2/143](https://doi.org/10.1088/0004-637X/809/2/143)
- Drimmel, R., Cabrera-Lavers, A., & López-Corredoira, M. 2003, *A&A*, 409, 205, doi: [10.1051/0004-6361:20031070](https://doi.org/10.1051/0004-6361:20031070)
- Ernandes, H., Feuillet, D., Feltzing, S., & Skúladóttir, Á. 2024, *A&A*, 691, A333, doi: [10.1051/0004-6361/202450827](https://doi.org/10.1051/0004-6361/202450827)
- Feldmeier-Krause, A. 2022, *MNRAS*, 513, 5920, doi: [10.1093/mnras/stac1227](https://doi.org/10.1093/mnras/stac1227)
- Feldmeier-Krause, A., Kerzendorf, W., Do, T., et al. 2020, *MNRAS*, 494, 396, doi: [10.1093/mnras/staa703](https://doi.org/10.1093/mnras/staa703)
- Feuillet, D. K., Feltzing, S., Sahlholdt, C., & Bensby, T. 2022, *ApJ*, 934, 21, doi: [10.3847/1538-4357/ac76ba](https://doi.org/10.3847/1538-4357/ac76ba)
- Feuillet, D. K., Sahlholdt, C. L., Feltzing, S., & Casagrande, L. 2021, *MNRAS*, 508, 1489, doi: [10.1093/mnras/stab2614](https://doi.org/10.1093/mnras/stab2614)
- Fukue, K., Matsunaga, N., Kondo, S., et al. 2021, *ApJ*, 913, 62, doi: [10.3847/1538-4357/abf0b1](https://doi.org/10.3847/1538-4357/abf0b1)
- Gaia Collaboration, Prusti, T., de Bruijne, J. H. J., et al. 2016, *A&A*, 595, A1, doi: [10.1051/0004-6361/201629272](https://doi.org/10.1051/0004-6361/201629272)
- Gaia Collaboration, Brown, A. G. A., Vallenari, A., et al. 2018, *A&A*, 616, A1, doi: [10.1051/0004-6361/201833051](https://doi.org/10.1051/0004-6361/201833051)
- . 2021, *A&A*, 649, A1, doi: [10.1051/0004-6361/202039657](https://doi.org/10.1051/0004-6361/202039657)
- Gaia Collaboration, Vallenari, A., Brown, A. G. A., et al. 2023, *A&A*, 674, A1, doi: [10.1051/0004-6361/202243940](https://doi.org/10.1051/0004-6361/202243940)
- Ghez, A. M., Duchêne, G., Matthews, K., et al. 2003, *ApJL*, 586, L127, doi: [10.1086/374804](https://doi.org/10.1086/374804)
- Gillessen, S., Plewa, P. M., Eisenhauer, F., et al. 2017, *ApJ*, 837, 30, doi: [10.3847/1538-4357/aa5c41](https://doi.org/10.3847/1538-4357/aa5c41)
- GRAVITY Collaboration, Abuter, R., Aymar, N., et al. 2022, *A&A*, 657, L12, doi: [10.1051/0004-6361/202142465](https://doi.org/10.1051/0004-6361/202142465)
- Green, G. M., Schlafly, E., Zucker, C., Speagle, J. S., & Finkbeiner, D. 2019, *ApJ*, 887, 93, doi: [10.3847/1538-4357/ab5362](https://doi.org/10.3847/1538-4357/ab5362)
- Guillard, N., Emsellem, E., & Renaud, F. 2016, *MNRAS*, 461, 3620, doi: [10.1093/mnras/stw1570](https://doi.org/10.1093/mnras/stw1570)
- Hamano, S., Ikeda, Y., Otsubo, S., et al. 2024, *PASP*, 136, 014504, doi: [10.1088/1538-3873/ad1b38](https://doi.org/10.1088/1538-3873/ad1b38)
- Hattori, K. 2025, *ApJ*, 980, 90, doi: [10.3847/1538-4357/ad9686](https://doi.org/10.3847/1538-4357/ad9686)
- Hattori, K., Okuno, A., & Roederer, I. U. 2023, *ApJ*, 946, 48, doi: [10.3847/1538-4357/acb93b](https://doi.org/10.3847/1538-4357/acb93b)
- Hattori, K., Valluri, M., Bell, E. F., & Roederer, I. U. 2018a, *ApJ*, 866, 121, doi: [10.3847/1538-4357/aadee5](https://doi.org/10.3847/1538-4357/aadee5)
- Hattori, K., Valluri, M., & Castro, N. 2018b, *ApJ*, 869, 33, doi: [10.3847/1538-4357/aaed22](https://doi.org/10.3847/1538-4357/aaed22)
- Hattori, K., Valluri, M., Castro, N., et al. 2019, *ApJ*, 873, 116, doi: [10.3847/1538-4357/ab05e8](https://doi.org/10.3847/1538-4357/ab05e8)
- Helmi, A., Babusiaux, C., Koppelman, H. H., et al. 2018, *Nature*, 563, 85, doi: [10.1038/s41586-018-0625-x](https://doi.org/10.1038/s41586-018-0625-x)
- Hidalgo, S. L., Pietrinferni, A., Cassisi, S., et al. 2018, *ApJ*, 856, 125, doi: [10.3847/1538-4357/aab158](https://doi.org/10.3847/1538-4357/aab158)
- Hills, J. G. 1988, *Nature*, 331, 687, doi: [10.1038/331687a0](https://doi.org/10.1038/331687a0)
- Horta, D., Schiavon, R. P., Mackereth, J. T., et al. 2021, *MNRAS*, 500, 1385, doi: [10.1093/mnras/staa2987](https://doi.org/10.1093/mnras/staa2987)
- . 2023, *MNRAS*, 520, 5671, doi: [10.1093/mnras/stac3179](https://doi.org/10.1093/mnras/stac3179)
- Hunter, J. D. 2007, *Computing in Science and Engineering*, 9, 90, doi: [10.1109/MCSE.2007.55](https://doi.org/10.1109/MCSE.2007.55)
- Ikeda, Y., Kondo, S., Otsubo, S., et al. 2022, *PASP*, 134, 015004, doi: [10.1088/1538-3873/ac1c5f](https://doi.org/10.1088/1538-3873/ac1c5f)
- Jin, S., Trager, S. C., Dalton, G. B., et al. 2023, *MNRAS*, doi: [10.1093/mnras/stad557](https://doi.org/10.1093/mnras/stad557)
- Jofré, E., Petrucci, R., Saffe, C., et al. 2015, *A&A*, 574, A50, doi: [10.1051/0004-6361/201424474](https://doi.org/10.1051/0004-6361/201424474)
- Jofré, P., Heiter, U., & Soubiran, C. 2019, *ARA&A*, 57, 571, doi: [10.1146/annurev-astro-091918-104509](https://doi.org/10.1146/annurev-astro-091918-104509)
- Jofré, P., Heiter, U., Tucci Maia, M., et al. 2018, *Research Notes of the American Astronomical Society*, 2, 152, doi: [10.3847/2515-5172/aadc61](https://doi.org/10.3847/2515-5172/aadc61)
- Kondo, S., Fukue, K., Matsunaga, N., et al. 2019, *ApJ*, 875, 129, doi: [10.3847/1538-4357/ab0ec4](https://doi.org/10.3847/1538-4357/ab0ec4)
- Koposov, S. E., Boubert, D., Li, T. S., et al. 2020, *MNRAS*, 491, 2465, doi: [10.1093/mnras/stz3081](https://doi.org/10.1093/mnras/stz3081)
- Kruijssen, J. M. D., Pfeffer, J. L., Reina-Campos, M., Crain, R. A., & Bastian, N. 2019, *MNRAS*, 486, 3180, doi: [10.1093/mnras/sty1609](https://doi.org/10.1093/mnras/sty1609)
- Levin, Y. 2007, *MNRAS*, 374, 515, doi: [10.1111/j.1365-2966.2006.11155.x](https://doi.org/10.1111/j.1365-2966.2006.11155.x)
- Li, T. S., Koposov, S. E., Zucker, D. B., et al. 2019, *MNRAS*, 490, 3508, doi: [10.1093/mnras/stz2731](https://doi.org/10.1093/mnras/stz2731)

- Li, Y.-B., Luo, A. L., Lu, Y.-J., et al. 2021, *ApJS*, 252, 3, doi: [10.3847/1538-4365/abc16e](https://doi.org/10.3847/1538-4365/abc16e)
- Marchetti, T. 2021, *MNRAS*, 503, 1374, doi: [10.1093/mnras/stab599](https://doi.org/10.1093/mnras/stab599)
- Marchetti, T., Contigiani, O., Rossi, E. M., et al. 2018, *MNRAS*, 476, 4697, doi: [10.1093/mnras/sty579](https://doi.org/10.1093/mnras/sty579)
- Marchetti, T., Evans, F. A., & Rossi, E. M. 2022a, arXiv e-prints, arXiv:2206.06962. <https://arxiv.org/abs/2206.06962>
- . 2022b, *MNRAS*, 515, 767, doi: [10.1093/mnras/stac1777](https://doi.org/10.1093/mnras/stac1777)
- Marchetti, T., Rossi, E. M., & Brown, A. G. A. 2019, *MNRAS*, 490, 157, doi: [10.1093/mnras/sty2592](https://doi.org/10.1093/mnras/sty2592)
- Marshall, D. J., Robin, A. C., Reyl e, C., Schultheis, M., & Picaud, S. 2006, *A&A*, 453, 635, doi: [10.1051/0004-6361:20053842](https://doi.org/10.1051/0004-6361:20053842)
- Matsunaga, N., Taniguchi, D., Jian, M., et al. 2020, *ApJS*, 246, 10, doi: [10.3847/1538-4365/ab5c25](https://doi.org/10.3847/1538-4365/ab5c25)
- McMillan, P. J. 2017, *MNRAS*, 465, 76, doi: [10.1093/mnras/stw2759](https://doi.org/10.1093/mnras/stw2759)
- Mel endez, J., & Barbuy, B. 1999, *ApJS*, 124, 527, doi: [10.1086/313261](https://doi.org/10.1086/313261)
- M esz aros, S., Allende Prieto, C., Edvardsson, B., et al. 2012, *AJ*, 144, 120, doi: [10.1088/0004-6256/144/4/120](https://doi.org/10.1088/0004-6256/144/4/120)
- Minelli, A., Mucciarelli, A., Romano, D., et al. 2021, *ApJ*, 910, 114, doi: [10.3847/1538-4357/abe3f9](https://doi.org/10.3847/1538-4357/abe3f9)
- Montegriffo, P., De Angeli, F., Andrae, R., et al. 2023, *A&A*, 674, A3, doi: [10.1051/0004-6361/202243880](https://doi.org/10.1051/0004-6361/202243880)
- Nandakumar, G., Ryde, N., Schultheis, M., et al. 2025, *ApJ*, arXiv:2502.17756. <https://arxiv.org/abs/2502.17756>
- Nandakumar, G., Ryde, N., Mace, G., et al. 2024, *ApJ*, 964, 96, doi: [10.3847/1538-4357/ad22dc](https://doi.org/10.3847/1538-4357/ad22dc)
- Neumayer, N., Seth, A., & B oker, T. 2020, *A&A Rv*, 28, 4, doi: [10.1007/s00159-020-00125-0](https://doi.org/10.1007/s00159-020-00125-0)
- Nishiyama, S., Yasui, K., Nagata, T., et al. 2013, *ApJL*, 769, L28, doi: [10.1088/2041-8205/769/2/L28](https://doi.org/10.1088/2041-8205/769/2/L28)
- Nishiyama, S., Kara, T., Thorsbro, B., et al. 2024, *Proceedings of the Japan Academy, Series B*, 100, 86, doi: [10.2183/pjab.100.007](https://doi.org/10.2183/pjab.100.007)
- Pfuhl, O., Fritz, T. K., Zilka, M., et al. 2011, *ApJ*, 741, 108, doi: [10.1088/0004-637X/741/2/108](https://doi.org/10.1088/0004-637X/741/2/108)
- Pietrinferni, A., Cassisi, S., Salaris, M., & Castelli, F. 2004, *ApJ*, 612, 168, doi: [10.1086/422498](https://doi.org/10.1086/422498)
- Piff, T., Binney, J., McMillan, P. J., et al. 2014, *MNRAS*, 445, 3133, doi: [10.1093/mnras/stu1948](https://doi.org/10.1093/mnras/stu1948)
- Portail, M., Gerhard, O., Wegg, C., & Ness, M. 2017, *MNRAS*, 465, 1621, doi: [10.1093/mnras/stw2819](https://doi.org/10.1093/mnras/stw2819)
- Portegies Zwart, S. F., McMillan, S. L. W., & Gieles, M. 2010, *ARA&A*, 48, 431, doi: [10.1146/annurev-astro-081309-130834](https://doi.org/10.1146/annurev-astro-081309-130834)
- Ram rez, S. V., Sellgren, K., Carr, J. S., et al. 2000, *ApJ*, 537, 205, doi: [10.1086/309022](https://doi.org/10.1086/309022)
- Reid, M. J., & Brunthaler, A. 2020, *ApJ*, 892, 39, doi: [10.3847/1538-4357/ab76cd](https://doi.org/10.3847/1538-4357/ab76cd)
- Rich, R. M., Ryde, N., Thorsbro, B., et al. 2017, *AJ*, 154, 239, doi: [10.3847/1538-3881/aa970a](https://doi.org/10.3847/1538-3881/aa970a)
- Ryabchikova, T., Piskunov, N., Kurucz, R. L., et al. 2015, *PhyS*, 90, 054005, doi: [10.1088/0031-8949/90/5/054005](https://doi.org/10.1088/0031-8949/90/5/054005)
- Ryde, N., Fritz, T. K., Rich, R. M., et al. 2016a, *ApJ*, 831, 40, doi: [10.3847/0004-637X/831/1/40](https://doi.org/10.3847/0004-637X/831/1/40)
- Ryde, N., Schultheis, M., Grieco, V., et al. 2016b, *AJ*, 151, 1, doi: [10.3847/0004-6256/151/1/1](https://doi.org/10.3847/0004-6256/151/1/1)
- Ryde, N., Nandakumar, G., Schultheis, M., et al. 2025, *ApJ*, 979, 174, doi: [10.3847/1538-4357/ad9b2b](https://doi.org/10.3847/1538-4357/ad9b2b)
- Sameshima, H., Matsunaga, N., Kobayashi, N., et al. 2018, *PASP*, 130, 074502, doi: [10.1088/1538-3873/aac1b4](https://doi.org/10.1088/1538-3873/aac1b4)
- Sch odel, R., Feldmeier, A., Neumayer, N., Meyer, L., & Yelda, S. 2014, *Classical and Quantum Gravity*, 31, 244007, doi: [10.1088/0264-9381/31/24/244007](https://doi.org/10.1088/0264-9381/31/24/244007)
- Sch onrich, R., Binney, J., & Dehnen, W. 2010, *MNRAS*, 403, 1829, doi: [10.1111/j.1365-2966.2010.16253.x](https://doi.org/10.1111/j.1365-2966.2010.16253.x)
- Schultheis, M., Rojas-Arriagada, A., Cunha, K., et al. 2020, *A&A*, 642, A81, doi: [10.1051/0004-6361/202038327](https://doi.org/10.1051/0004-6361/202038327)
- Schultheis, M., Fritz, T. K., Nandakumar, G., et al. 2021, *A&A*, 650, A191, doi: [10.1051/0004-6361/202140499](https://doi.org/10.1051/0004-6361/202140499)
- Snedden, C. 1973, *ApJ*, 184, 839, doi: [10.1086/152374](https://doi.org/10.1086/152374)
- Snedden, C., Bean, J., Ivans, I., Lucatello, S., & Sobek, J. 2012, MOOG: LTE line analysis and spectrum synthesis, *Astrophysics Source Code Library*, record ascl:1202.009. <http://ascl.net/1202.009>
- Steinmetz, M., Guiglion, G., McMillan, P. J., et al. 2020, *AJ*, 160, 83, doi: [10.3847/1538-3881/ab9ab8](https://doi.org/10.3847/1538-3881/ab9ab8)
- Suda, T., Katsuta, Y., Yamada, S., et al. 2008, *PASJ*, 60, 1159, doi: [10.1093/pasj/60.5.1159](https://doi.org/10.1093/pasj/60.5.1159)
- Takada, M., Ellis, R. S., Chiba, M., et al. 2014, *PASJ*, 66, R1, doi: [10.1093/pasj/pst019](https://doi.org/10.1093/pasj/pst019)
- Taniguchi, D., Matsunaga, N., Kobayashi, N., et al. 2018, *MNRAS*, 473, 4993, doi: [10.1093/mnras/stx2691](https://doi.org/10.1093/mnras/stx2691)
- Taniguchi, D., Matsunaga, N., Jian, M., et al. 2021, *MNRAS*, 502, 4210, doi: [10.1093/mnras/staa3855](https://doi.org/10.1093/mnras/staa3855)
- Taniguchi, D., Matsunaga, N., Kobayashi, N., et al. 2025, *A&A*, 693, A163, doi: [10.1051/0004-6361/202452392](https://doi.org/10.1051/0004-6361/202452392)
- Van der Swaelmen, M., Hill, V., Primas, F., & Cole, A. A. 2013, *A&A*, 560, A44, doi: [10.1051/0004-6361/201321109](https://doi.org/10.1051/0004-6361/201321109)
- van der Walt, S., Colbert, S. C., & Varoquaux, G. 2011, *Computing in Science Engineering*, 13, 22, doi: [10.1109/MCSE.2011.37](https://doi.org/10.1109/MCSE.2011.37)
- Vasiliev, E. 2019, *MNRAS*, 482, 1525, doi: [10.1093/mnras/sty2672](https://doi.org/10.1093/mnras/sty2672)

- Verberne, S., Rossi, E. M., Kuposov, S. E., et al. 2024, MNRAS, 533, 2747, doi: [10.1093/mnras/stae1888](https://doi.org/10.1093/mnras/stae1888)
- Virtanen, P., Gommers, R., Oliphant, T. E., et al. 2020, Nature Methods, 17, 261, doi: [10.1038/s41592-019-0686-2](https://doi.org/10.1038/s41592-019-0686-2)
- Zhang, F., Lu, Y., & Yu, Q. 2013, ApJ, 768, 153, doi: [10.1088/0004-637X/768/2/153](https://doi.org/10.1088/0004-637X/768/2/153)
- Zhang, X., Green, G. M., & Rix, H.-W. 2023, MNRAS, 524, 1855, doi: [10.1093/mnras/stad1941](https://doi.org/10.1093/mnras/stad1941)
- Zhao, G., Zhao, Y., Chu, Y., Jing, Y., & Deng, L. 2012, arXiv e-prints, arXiv:1206.3569, <https://arxiv.org/abs/1206.3569>

Table 6. Chemical abundances of WINERED-HVS1 measured with the VALD3 line list (Ryabchikova et al. 2015)

v_{micro} [km s ⁻¹]	1.364 ^{+0.154} _{-0.147}	
[Fe/H] [dex]	-0.118 ^{+0.042} _{-0.044} (43)	
	[X/H] [dex]	[X/Fe] [dex]
Na I	—	—
Mg I	-0.151 ^{+0.148} _{-0.145}	-0.033 ^{+0.157} _{-0.155} (2)
Si I	+0.086 ^{+0.079} _{-0.072}	+0.204 ^{+0.079} _{-0.082} (17)
S I	+0.191 ^{+0.297} _{-0.276}	+0.309 ^{+0.291} _{-0.278} (1)
K I	—	—
Ca I	-0.075 ^{+0.167} _{-0.167}	+0.043 ^{+0.171} _{-0.173} (8)
Ti I	-0.135 ^{+0.146} _{-0.147}	-0.018 ^{+0.146} _{-0.157} (12)
Cr I	-0.127 ^{+0.130} _{-0.129}	-0.009 ^{+0.133} _{-0.138} (9)
Ni I	+0.007 ^{+0.147} _{-0.146}	+0.125 ^{+0.148} _{-0.148} (2)
Sr II	-0.125 ^{+0.236} _{-0.232}	-0.007 ^{+0.236} _{-0.235} (1)

APPENDIX

A. SPECTRAL ANALYSIS USING A DIFFERENT LINE LIST

In the main part of this paper, we use the MB99 line list (Meléndez & Barbuy 1999) to derive the chemical abundances of WINERED-HVS1. Table 6 shows the same result but using the VALD3 line list (Ryabchikova et al. 2015).

B. A MONTE CARLO SIMULATION OF HYPER-VELOCITY STARS

B.1. Empirical model of Hills mechanism

According to the theoretical investigations by Hills (1988) and Bromley et al. (2006), the typical ejection velocity of a HVS due to the Hills mechanism—involving the 3-body interaction between a SMBH (with mass M_{BH}) and a stellar binary (consisting of two stars separated by a semi-major axis a with masses of m_1 and m_2)—is given by the equation:

$$v_{\text{ej}} = 1370 \text{ km s}^{-1} \left(\frac{a}{0.1 \text{ AU}} \right)^{-1/2} \left(\frac{m_1 + m_2}{M_{\odot}} \right)^{1/2} \left(\frac{M_{\text{BH}}}{4 \times 10^6 M_{\odot}} \right)^{1/6} f_R. \tag{B1}$$

In this equation, v_{ej} represents the typical velocity of the escaping star once it has left the gravitational influence of the SMBH (approximately at a distance of 1 parsec from the SMBH). In the main part of this paper, we employ two models of the Galactic gravitational potential that do not account for the SMBH’s potential. Therefore, the ejection velocity v_{ej} computed in the main text for stars in the Gaia catalog can be directly compared with the value of v_{ej} provided in equation (B1).

We note that the empirical factor $f_R < 1$ is of order unity and depends on the dimensionless quantity

$$D = \frac{r_{\text{peri}}}{a} \left(\frac{10^6 M_{\odot}}{M_{\text{BH}}} \frac{m_1 + m_2}{2M_{\odot}} \right)^{1/3}. \tag{B2}$$

In this equation, r_{peri} represents the closest approach distance between the binary system and the SMBH. The approximate formula for $f_R(D)$ provided by Bromley et al. (2006) is

$$f_R(D) = \sum_{k=0}^5 c_k D^k \quad (\text{for } 0 \leq D \leq 175) \tag{B3}$$

with coefficients given by $(c_0, c_1, c_2, c_3, c_4, c_5) = (0.774, 0.0204, -6.23 \times 10^{-4}, 7.62 \times 10^{-6}, -4.24 \times 10^{-8}, 8.62 \times 10^{-11})$. The quantity D also governs the empirical ejection probability, which can be expressed as

$$P_{\text{ej}} = \begin{cases} 1 - \frac{D}{175} & (\text{for } 0 \leq D \leq 175), \\ 0 & (\text{otherwise}). \end{cases} \tag{B4}$$

B.2. A Monte Carlo simulation of $2M_{\odot}$ HVSs

In the main analysis of this paper, we find that WINERED-HVS1, along with other metal-rich HVS candidates, has an estimated mass of approximately $2M_{\odot}$ based on its location in the CMD. To understand the physical parameters that lead to the ejection of a $2M_{\odot}$ star with an ejection velocity ranging from 500 to 600 km s^{-1} , we perform a Monte Carlo simulation consisting of $n_{\text{MC}} = 5 \times 10^5$ realizations. In the following analysis, we will assume that $M_{\text{BH}} = 4 \times 10^6 M_{\odot}$ and that both stars in the binary have a mass of $m_1 = m_2 = 2M_{\odot}$.

Following Bromley et al. (2006), we assume that the binary’s closest approach to the SMBH satisfies the condition $1 \text{ AU} < r_{\text{peri}} < 700 \text{ AU}$. To simplify our calculations, we assume that r_{peri} is equal to the impact parameter of the center-of-mass orbit of the binary at infinity. In this context, the probability of having the impact parameter between r_{peri} and $r_{\text{peri}} + dr_{\text{peri}}$ is proportional to $2\pi r_{\text{peri}} dr_{\text{peri}}$. We randomly sample n_{MC} values of r_{peri} from the range $1 \text{ AU} < r_{\text{peri}} < 700 \text{ AU}$ according to this probability distribution.

Additionally, following Bromley et al. (2006), we assume that the logarithmic value of the binary’s semi-major axis, $\ln a$, follows a uniform distribution. The lower limit for a is set at 0.02 AU, which is the minimum allowed value of a so that two $2M_{\odot}$ main-sequence stars in a binary do not merge.¹⁹ The upper limit for a is set at 100 AU, which is sufficiently large that our analysis is not sensitive to this value. We also randomly sample n_{MC} values of a according to this probability distribution.

For each pair (a, r_{peri}) , we calculate three quantities: D , the ejection velocity v_{ej} , and the ejection probability P_{ej} . If P_{ej} is non-zero, we store the corresponding v_{ej} . Out of $n_{\text{MC}} = 5 \times 10^5$ realizations, we find that 2457 realizations result in an ejection with $v_{\text{ej}} = 500\text{--}600 \text{ km s}^{-1}$. The fraction of ejections within this range of v_{ej} is small, mainly because the upper limit for a is set very high. Under our current assumptions, no HVSs would be ejected with $v_{\text{ej}} > 500 \text{ km s}^{-1}$ if $a > 3 \text{ AU}$ is satisfied.

Fig. 6 illustrates the results of this analysis. For a HVS with a mass of $2M_{\odot}$, achieving an ejection velocity of 500–600 km s^{-1} typically requires $a \sim 2.06 \text{ AU}$ (median) and $r_{\text{peri}} \simeq 170 \text{ AU}$ (median). The values of a and r_{peri} can vary by a factor of around 2. For $a > 1.4 \text{ AU}$, the Roche radius of an equal-mass binary satisfies $R_{\text{Roche}} = 0.38a > 0.5 \text{ AU}$. Given that the radius of a $2M_{\odot}$ red giant is typically smaller than 0.5 AU, a condition of $a > 1.4 \text{ AU}$ is a sufficient condition for a binary system consisting of two $2M_{\odot}$ red giants does not merge. In this regard, it is noteworthy that the majority (92%) of the Monte Carlo realizations that yielded $v_{\text{ej}} = 500\text{--}600 \text{ km s}^{-1}$ satisfy the condition $a > 1.4 \text{ AU}$. Our result indicates that a binary system consisting of two $2M_{\odot}$ red giant stars can interact with the Galactic SMBH to produce a red-giant HVS with an ejection velocity of 500–600 km s^{-1} , depending on the value of r_{peri} . This result is intriguing, as WINERED-HVS1 is a metal-rich red giant with a mass of $\sim 2M_{\odot}$.

While our primary focus is on HVSs with $v_{\text{ej}} = 500\text{--}600 \text{ km s}^{-1}$, our Monte Carlo simulation also provides some insights into HVSs with higher or lower ejection velocities. As demonstrated in Fig. 6, higher ejection velocities for HVSs with a mass of $2M_{\odot}$ generally require lower values of r_{peri} and smaller a . This result is reasonable because a binary can acquire significant kinetic energy at r_{peri} if the value of r_{peri} is smaller; and such an close encounter requires a tightly bound binary system, resulting in smaller values of a .

C. PROPERTIES OF OUR HVS CANDIDATE AND THE THEORETICAL PREDICTIONS

In this paper, we identify 22 HVS candidates, and one of the candidates, WINERED-HVS1, is a promising candidate in terms of its chemistry. Here we investigate whether our discovery of one HVS (candidate) from the Gaia catalog is statistically natural or not.

C.1. Basic properties of WINERED-HVS1

First, we ignore the fact that this star is an HVS candidate and investigate the other observational properties (such as its magnitude) of WINERED-HVS1 from a statistical perspective. Based on the Gaia DR3 catalog, its G_{RP} , G , and G_{RVS} magnitudes are $G_{\text{RP}} = 13.58$, $G = 14.28$, and $G_{\text{RVS}} = 13.26$. Among 1.7 billion stars in the Gaia DR3, only 1% of them have G_{RP} or G values that are brighter than WINERED-HVS1. Also, among 219 million stars with Gaia XP spectra, only 9% of them have G_{RP} or G values that are brighter than WINERED-HVS1. These numbers indicate that WINERED-HVS1 is a bright object. However, except for its brightness, WINERED-HVS1 is not particularly special. By randomly selecting stars with similar G_{RP} magnitudes ($13.56 < G_{\text{RP}} < 13.60$), we find 91% of them have Gaia XP spectra, 88% have line-of-sight velocity (v_{los}) measurements by Gaia, 87% have good parallax measurements ($\text{parallax_over_error} > 5$), and 74% satisfy all the criteria above (as WINERED-HVS1 does). The fractions are almost identical if we select stars based on G -magnitude ($14.26 < G < 14.30$) instead.

¹⁹ The Roche radius of an equal-mass binary is given by $R_{\text{Roche}} = 0.38a$. By equating the Roche radius and the radius of a $2M_{\odot}$ main-sequence star ($\sim 0.008 \text{ AU}$), we obtain the minimum allowed value of a .

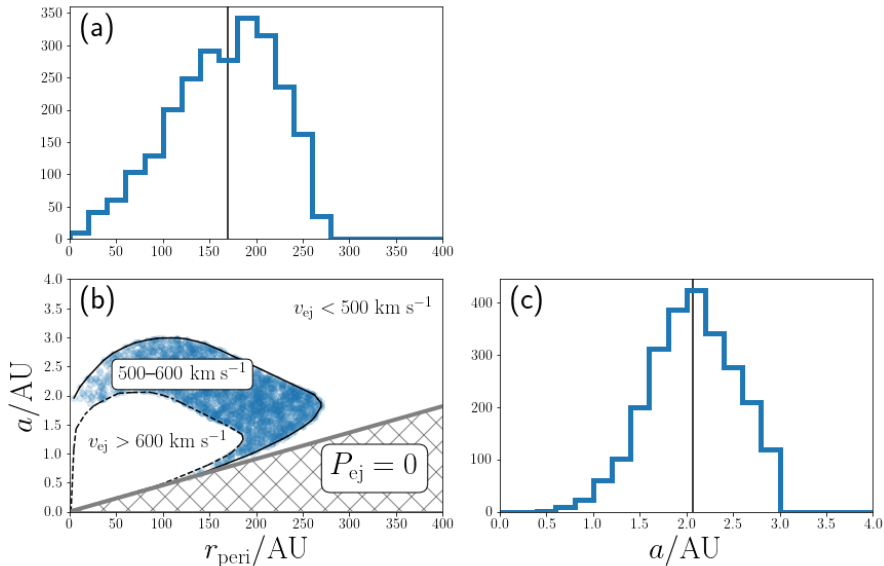


Figure 6. The result of Monte Carlo simulation of HVSs with a mass of $2M_{\odot}$. In panel (b), the blue dots shows the distribution of (r_{peri}, a) that allows the ejection of a $2M_{\odot}$ HVS to attain ejection velocity of $500\text{--}600\text{ km s}^{-1}$. The hatched region corresponds to a parameter subspace where no ejection happens ($P_{\text{ej}} = 0$; $D > 175$). Higher (lower) ejection velocities are attained for smaller (larger) r_{peri} and a . Other panels shows the marginalized distributions of the blue points in panel (b).

C.2. Complications in the mock HVS catalog in Marchetti et al. (2018)

Marchetti et al. (2018) predicted the populations of HVSs observable in the Gaia catalog. Their HILLS mock catalog is a simulated catalog of both bound and unbound HVSs ejected from the Galactic center, assuming an HVS ejection rate of $2.8 \times 10^{-4}\text{ yr}^{-1}$. Since WINERED-HVS1 is identified as a bound HVS candidate, their HILLS catalog is appropriate for comparison with our results. However, before using their results, we must clarify three key differences between their identification of HVSs in the simulation and our search for HVS candidates.

(Complication 1): We selected HVS candidates from a catalog of 48 million stars in Hattori (2025). In creating this catalog, Hattori (2025) did not use the full list of stars with Gaia XP spectra, which consists of 219 million stars. Instead, he focused on the 48 million stars located in regions with low dust extinction with $E(B - V) < 0.1$. Consequently, our search for HVSs is inevitably restricted to those HVSs in regions with low dust extinction. In contrast, Marchetti et al. (2018) used a 3D dust extinction map to generate dust-obscured photometric data for their simulated HVSs. Their synthetic data included HVSs from both high and low dust extinction regions. If we crudely assume that the spatial distribution of stars with Gaia XP spectra is similar to that of the HVSs,²⁰ we can estimate that we are searching for HVSs from approximately 22% of the available data (48 million/219 million).

(Complication 2): Since Marchetti et al. (2018) only estimated the expected number of main-sequence HVSs, we need to be careful when using their mock catalog to assess the likelihood of discovering a red-giant HVS, such as WINERED-HVS1. The key differences between main-sequence HVSs and red-giant HVSs (with the same initial masses) are that the main-sequence phase lasts longer, and a red giant is intrinsically brighter. According to the Padova isochrone model (Bressan et al. 2012), a $\sim 2M_{\odot}$ main-sequence star becomes approximately 1 mag brighter when it evolves into a red giant. Additionally, the duration of the red-giant phase is only 21% of the main-sequence phase for a star with an initial mass of $2M_{\odot}$. An increase of brightness by 1 mag allows a magnitude-limited survey to cover 2.5 times larger distances and 16 ($= 2.5^3$) times larger volumes. Fig. 8 of Marchetti et al. (2018) predicted ~ 95 main-sequence HVSs with $G_{\text{RVS}} < 13.26$ (as bright as or brighter than WINERED-HVS1) and ~ 380 main-sequence HVSs with $G_{\text{RVS}} < 14.26$ (which extends the upper limit by 1 mag). Thus, in their analysis, increasing the G_{RVS} by 1 mag results in a 4 ($= 380/95$) times larger number of main-sequence HVSs. Based on these arguments, we expect that an increase of 1 mag in HVS brightness may lead to an increase in its detectability by a factor of 4 to 16. Considering

²⁰ This approximation may not be as inaccurate as it seems. Most of the stars with Gaia XP spectra are disk stars and have a flattened distribution. The spatial distribution of HVSs in the left panel of Fig. 10 from Marchetti et al. (2018) also appears slightly oblate (even after accounting for the figure’s aspect ratio). This flattened distribution may be due to bound HVSs being drawn toward the Galactic mid-plane because of the gravitational pull from the stellar disk.

the short duration of the red-giant phase, we estimate that the detectability of a $2-M_{\odot}$ red-giant HVS may be around 0.8–3.4 ($= 0.21 \times (4-16)$) times that of a main-sequence HVS with the same mass.

(Complication 3): In this paper, we aimed to identify HVSs that have recently been ejected from the Galactic center. Specifically, we searched for unbound HVSs and recently ejected bound HVSs that have not yet crossed the Galactic disk after the ejection. In contrast, the simulated HVSs described in [Marchetti et al. \(2018\)](#) also included bound HVSs with one or more disk crossings after the ejection. Based on our analysis in [Table 3](#), the typical flight time for recently ejected HVSs is approximately 20 Myr. Therefore, we effectively exclude HVSs with longer flight times, and we need to account for this factor in our analysis. Given the following points: (i) HVS ejections can occur at any time during a star’s lifetime, (ii) the estimated lifetime of WINERED-HVS1 is $\sim 0.5-10$ Gyr, and (iii) the typical flight time of recently ejected HVSs is ~ 20 Myr, it can be inferred that identifying one recently ejected HVS candidate (WINERED-HVS1) may suggest the existence of $\sim 25-500$ ($= 0.5-10$ Gyr/20 Myr) bound HVSs with similar characteristics to WINERED-HVS1 in our input catalog.

C.3. Assessment of the likelihood to find one red-giant HVS

Despite the complications mentioned above, we dare to explore how our discovery of one HVS (candidate) can be interpreted in the context of the theoretical predictions made by [Marchetti et al. \(2018\)](#). Since [Marchetti et al. \(2018\)](#) only considered main-sequence HVSs, we first pretend as if we found a ‘main-sequence’ HVS with $G_{\text{RVS}} = 13.26$.

As predicted in Fig. 8 of [Marchetti et al. \(2018\)](#), we assume that there are ~ 95 main-sequence HVSs with $G_{\text{RVS}} < 13.26$ (i.e., at least as bright as WINERED-HVS1). Also, we assume that 74% of Gaia stars with this same magnitude range possess Gaia XP spectra, v_{los} , and reliable parallax measurements (see [Section C.1](#)), and that 22% of HVSs are found in low dust extinction regions (see (Complication 1)). Then we expect to identify ~ 15 ($= 95 \times 0.74 \times 0.22$) main-sequence HVSs that meet the following criteria: (i) $G_{\text{RVS}} < 13.26$, (ii) located in low dust extinction regions ($E(B - V) < 0.1$), and (iii) possessing the Gaia XP spectra, velocity measurements, and reliable parallax.

As noted in (Complication 2), what we found is a $2-M_{\odot}$ red-giant HVS candidate (WINERED-HVS1), which is more likely to be detected by a factor of 0.8–3.4 than a main-sequence HVS with the same mass. Furthermore, as discussed in (Complication 3), what we searched for were recently ejected HVSs, which may consist of $\sim 1/500-1/25$ of the entire HVS population with similar properties. After correcting for these factors, the expected number of bound red-giant HVSs is 0.02–2. Therefore, finding one HVS candidate from our input catalog may be consistent with theoretical prediction.

Additionally, their Fig. 11 (top panel) and Fig. 7 indicate that the majority of HVSs with $G_{\text{RVS}} < 16$ have total velocities of $v < 500$ km s $^{-1}$ and are located at the Galactocentric distances of $r < 10$ kpc. These findings are consistent with WINERED-HVS1, which has a velocity of $v = 273$ km s $^{-1}$ and is located at $r = 5.45$ kpc. These characteristics suggest that the HVS candidate we identified may represent a typical bound HVS in the Gaia data.

D. ORBITAL PROPERTIES OF METAL-RICH HVS CANDIDATES

In the main part of this paper, we show the properties of WINERED-HVS1 (Fig. 3). Here, we show the orbital properties of the other HVS candidates. We show the plots for spectroscopically confirmed metal-rich HVS candidates (mrHVSsp1-9) in Figs. 7 and 8. We show the plots for XP-based metal-rich HVS candidates (mrHVSxp2-13) in Figs. 9, 10, and 11.

E. NOTATIONS IN THIS PAPER

[Table 7](#) summarizes the notations for astrometric quantities and chemical abundances used in this paper.

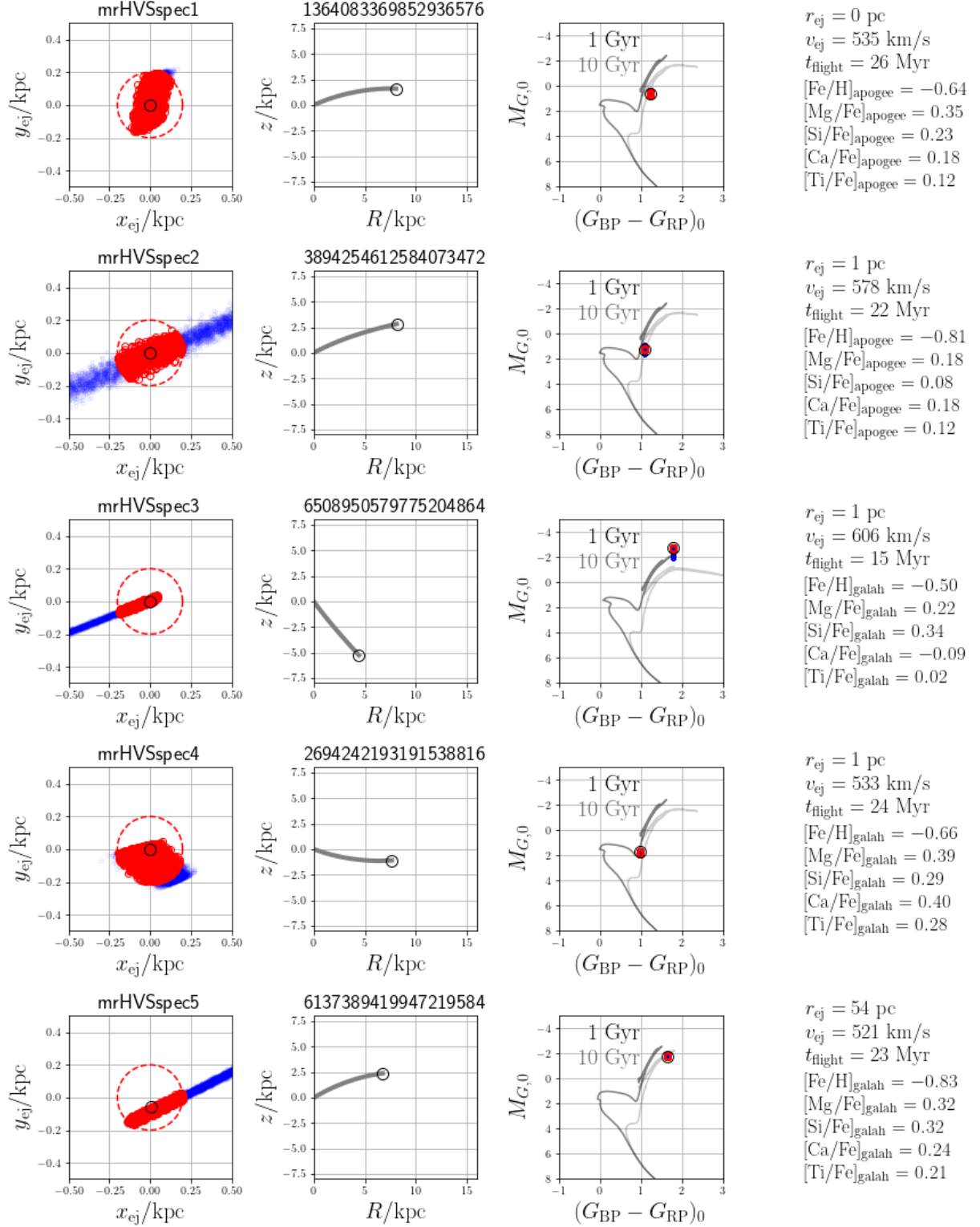


Figure 7. The same as Fig. 3 but for mrHVSspec1-5.

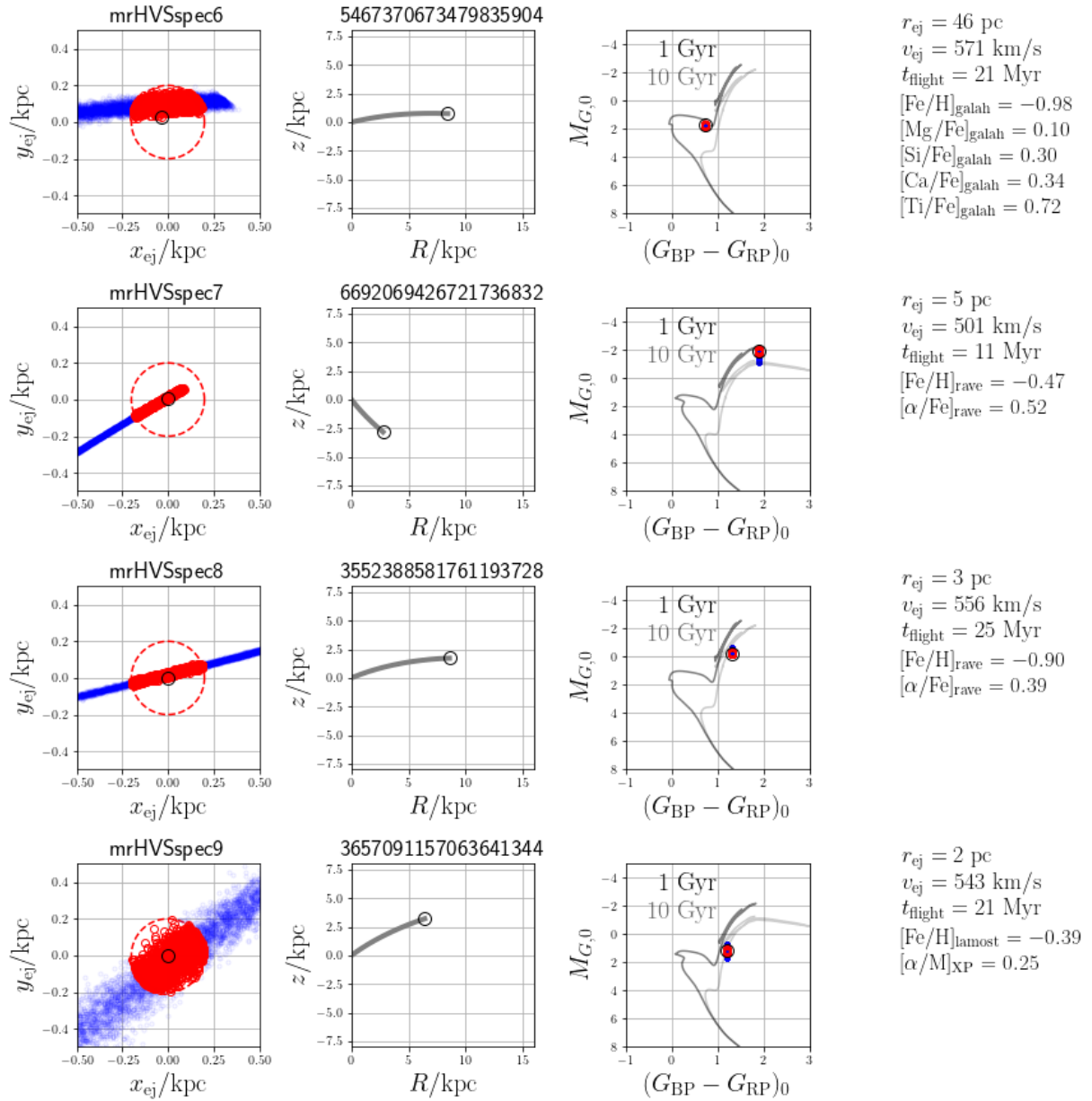


Figure 8. The same as Fig. 3 but for mrHVSspec6-9.

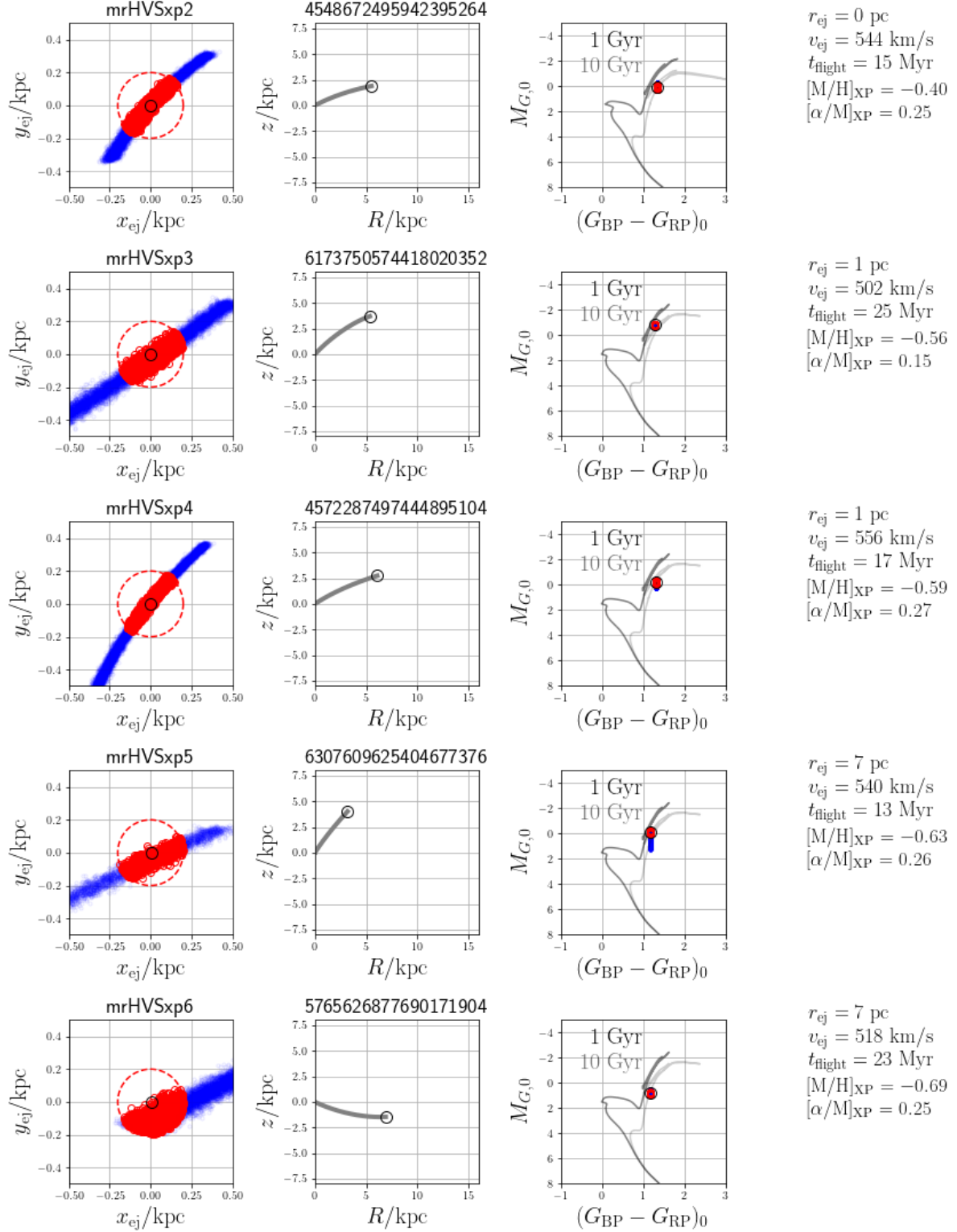


Figure 9. The same as Fig. 3 but for mrHVSxp2-6.

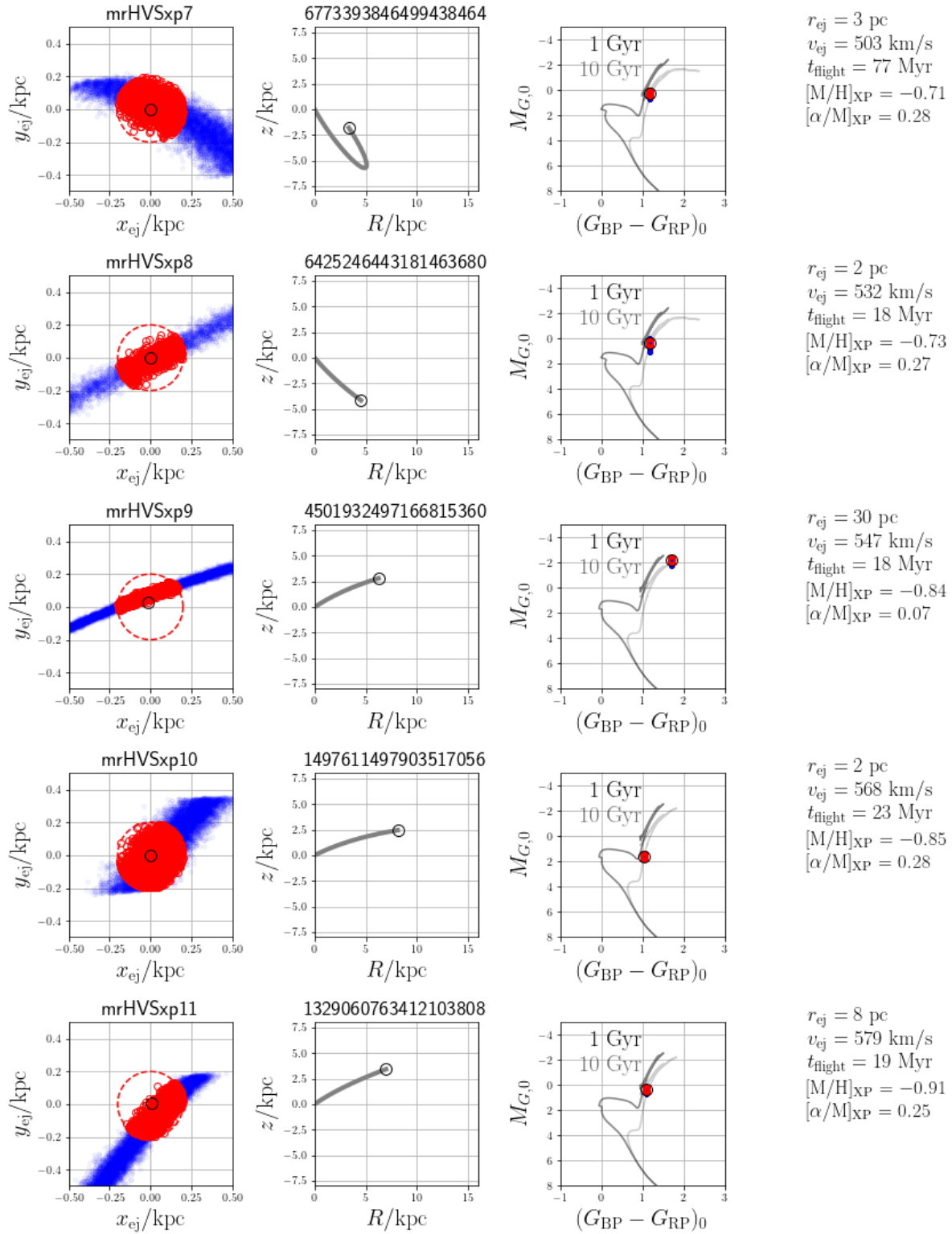


Figure 10. The same as Fig. 3 but for mrHVSxp7-11.

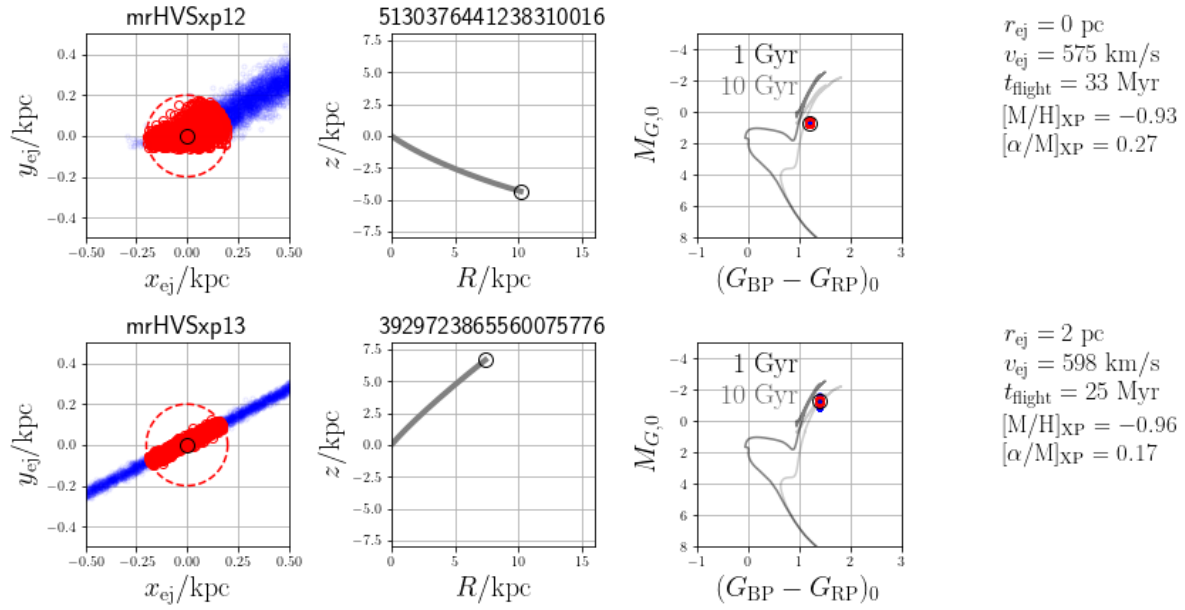


Figure 11. The same as Fig. 3 but for mrHVSxp12-13.

Table 7. Notations in this paper

Quantity	Meaning
α	Right ascension
δ	Declination
d	Heliocentric distance
ϖ	Parallax
σ_{ϖ}	Parallax error
$\mu_{\alpha*}$	Proper motion in α
μ_{δ}	Proper motion in δ
v_{los}	Heliocentric line-of-sight velocity
$[M/H]_{\text{XP}}$	Metallicity $[M/H]$ determined from Gaia XP spectra (Hattori 2025)
$[\alpha/M]_{\text{XP}}$	α -abundance $[\alpha/M]$ determined from Gaia XP spectra (Hattori 2025)
$[X/Y]_{\text{spec}}$	Spectroscopically determined chemical abundance $[X/Y]$
$[\alpha/Fe]_{\text{spec}}$	Spectroscopically determined α -abundance. ^(a)

NOTE— (a) If $[\alpha/Fe]_{\text{spec}}$ is in the literature (e.g., mrHVSspec7-8 or S0-6/S10), we use the literature value. If not, we compute $[\alpha/Fe]_{\text{spec}}$ from available abundance ratios of α elements. If four abundance ratios $[Mg/Fe]$, $[Si/Fe]$, $[Ca/Fe]$, and $[Ti/Fe]$ are available, we compute the average and standard deviation of these four values and use them as $[\alpha/Fe]_{\text{spec}}$ and the associated uncertainty. (In computing these average, we ignore the uncertainties in each abundance ratios. For example, we ignore the uncertainty in $[Mg/Fe]$.) If only some of the four ratios are available, we take the average and standard deviation of the available ratios.